

Palladium, Yttrium, Copper Ternary Alloys for Hydrogen
Purification

By
Joanne Louise Grant

A thesis submitted to the University of Birmingham for the
degree of
MASTER OF RESEARCH

Department of Metallurgy and Materials
School of Engineering
University of Birmingham
September 2009

UNIVERSITY OF
BIRMINGHAM

University of Birmingham Research Archive

e-theses repository

This unpublished thesis/dissertation is copyright of the author and/or third parties. The intellectual property rights of the author or third parties in respect of this work are as defined by The Copyright Designs and Patents Act 1988 or as modified by any successor legislation.

Any use made of information contained in this thesis/dissertation must be in accordance with that legislation and must be properly acknowledged. Further distribution or reproduction in any format is prohibited without the permission of the copyright holder.

Abstract

Palladium has long been recognised for its hydrogen sorption and separation capabilities. Alloying with different metals to produce binary alloys has been shown to further improve many of its essential properties significantly.

Currently palladium-silver alloys are used commercially for the hydrogen purification process, however, other binary alloys have also been shown to significantly improve the hydrogen sorption properties (palladium-yttrium), and palladium's resistance to poisoning by hydrogen sulphide (palladium-copper).

Whilst a number of binary palladium alloys have previously been investigated none has shown all the required target properties for an effective hydrogen purification membrane as set by the US DoE .

This work will study a number of palladium, yttrium, copper, ternary alloys of varying copper compositions, and investigate their characteristics as a suitable hydrogen purification material. The produced membranes, will be characterised using X-ray diffraction, scanning electron microscopy, hardness measurements, and the use of a confocal microscope and then tested using a hydrogen flow rig, to determine their suitability as a hydrogen purification material.

Results showed that the addition of a small amount of copper to a Pd-8at%Y alloy leads to marked changes in a number of key alloy parameters relevant to membrane performance. The lattice parameter was increased, as was hydrogen flow, and materials hardness, whilst average grain size was reduced.

Acknowledgements

Firstly I would like to thank the EPSRC for making the funding available for me to complete my course

Secondly I would like to thank both David Book and John Speight for there supervision, support and guidance throughout my time studying.

Thanks to Sean Fletcher for his time and help to me throughout my studies, and to the many others from the department that have offered guidance to me throughout my work.

Many thanks must also go to my parents and sister, who encouraged me to return to studying and follow this interest, and have continued to support me throughout the year of study and time writing up.

And finally many thanks to the friends I have made both in the lab and the Department that helped make the year so enjoyable.

Contents

1.0 Introduction	1
1.1 Hydrogen Production.....	4
1.1.1 Steam Methane Reforming (SMR)/Steam reforming of natural gas.....	4
1.1.2 Hydrogen Production from coal (Coal Gasification).....	4
1.1.3 Burning of Biomass.....	5
1.1.4 Electrolysis of water.....	6
1.2 Hydrogen in Transport.....	6
1.2.1 Internal Combustion Engines (ICEs).....	6
1.2.2 Fuel Cells.....	7
1.2.2.1 Proton Exchange Membrane Fuel Cells.....	7
2.0 Literature Review.....	10
2.1 Methods of hydrogen purification	10
2.1.1 Pressure Swing Absorption.....	10
2.1.2 Porous Material Membranes.....	10
2.1.3 Palladium Based Membranes (Metal Membranes).....	11
2.2 Metallic Membranes.....	12
2.3 Palladium for hydrogen purification.....	12
2.3.1 Hydrogen Flux.....	13
2.3.1.1 Guidelines and targets for a suitable hydrogen purification membrane.....	15
2.3.2 Contamination and Poisoning.....	16
2.3.2.1 Effect of Carbon Monoxide (CO)	17
2.3.2.2 Effect of Hydrogen Sulphide (H ₂ S).....	17
2.3.3 Methods of Membrane Fabrication.....	18
2.3.3.1 Rolling.....	18
2.3.3.2 Sputtering.....	19
2.3.3.2.1 Magnetron sputtering.....	19
2.3.3.3 Electroplating.....	20
2.3.3.4 Electroless plating.....	20
2.4 Binary Palladium Alloys.....	21
2.4.1 Palladium Silver.....	21
2.4.2 Palladium Yttrium.....	23
2.4.2.1 Solid Solubility.....	24
2.4.1.2 Hardness and Strength.....	25
2.4.2.3 Hydrogen Permeability.....	26
2.4.2.4 Effect of Order.....	29
2.4.3 Palladium-Copper.....	30
2.4.3.1 The effect of crystal structure.....	31
2.4.3.2 Hydrogen Permeability.....	32
2.4.3.3 Resistance to Sulphur.....	33
2.5 Palladium Ternary and More Complex Alloys.....	34
2.5.1 Palladium-Yttrium (Gadolinium)-Silver.....	34
2.5.2 Palladium-Yttrium-Indium (Tin, Lead).....	34
2.5.3 Palladium-Yttrium-Copper.....	35

2.6 Summary.....	36
2.7 Aims and Objectives.....	37
3.0 Experimental.....	38
3.1 Sample Preparation.....	38
3.2 Materials Characterisation.....	38
3.2.1 X-ray diffraction (XRD).....	38
3.2.2 Scanning electron microscopy (SEM).....	40
3.2.2.1 Energy Dispersive Spectrometer (EDS).....	40
3.2.3 Hardness Measurements.....	41
3.2.4 Confocal Microscope.....	41
3.3 Materials Testing.....	42
3.3.1 Hydrogen Flow Rig.....	42
4.0 Results.....	44
4.1 Initial Observations.....	44
4.2 X-Ray Diffraction.....	45
4.3 SEM and EDS analysis.....	54
4.4 Materials Hardness.....	64
4.5 Microstructural/ Micrographic Analysis.....	69
4.6 Hydrogen flux.....	78
4.7 Cost Analysis.....	80
4.8 General Discussion.....	82
5.0 Conclusion.....	85
6.0 Further Work.....	87
References.....	89

1.0 INTRODUCTION

Energy is essential for our current lifestyle, whether it is used in heating, lighting, the running of everyday electrical equipment or transportation. As advances are made in technology, demand for energy increases. At present, the UK consumes approximately 350 TWh of electricity annually.¹

Today the majority of our energy demands are met through the burning of fossil fuels to produce electricity and for transportation. However, whilst these non-renewable fuels have been our main energy source for a number of years they are limited in supply. Although estimates vary considerably, recent predictions suggest remaining supplies of coal will be exhausted within 164 years,² whilst reserves for oil and gas are lower still at 41 years and 67 years² respectively.

In addition to the uncertainties created by these predictions, the environmental effects caused by the release of CO₂ when fossil fuels are burnt to release energy are also of increasing concern. The negotiation of the Kyoto protocol in 1997, with the objective of reducing CO₂ emissions along with emissions of other greenhouse gases which are linked to global warming, must also be considered. For these reasons the continuing research that is underway to find an alternative, renewable, sustainable and environmentally friendly energy source is essential.

Alternative energy sources are available in the form of nuclear power, and renewable sources including solar, wind, and hydropower. However, at present more than three quarters of UK electricity generation comes from fossil fuels (Figure 1),³ whilst approximately 15% is

generated from nuclear and less than 7% is generated from renewable sources (Figure 1). In addition the use of fossil fuels to generate electricity, oil is also required for transportation. At present 66% of UK oil demand is derived from the demand for transportation fuels.⁴

Several options are being explored in an effort to reduce the need for oil for transportation. A variety of vehicles has already been produced including electric vehicles, hybrid vehicles, and vehicles which run off biomass.

Electric vehicles - run using an electric motor which can efficiently convert 75% of the battery's chemical power to power the vehicle. This process produces no pollutants from the vehicle, however, these vehicles have a short range at around half that of a petrol fuelled vehicle, they also take several hours to recharge⁵, whilst the battery can be expensive, heavy and take up considerable space.

*Hybrid vehicles*⁶ – have a smaller cheaper battery than electric vehicles with a longer range and more manageable lifetime. However, the need for an internal combustion engine (ICE) means efficiency is incremental and that the car is 100% dependant on oil.

Biofuel vehicles – may run off a variety of fuels produced from dead biological material although the most common biofuels are derived from photosynthetic plants. However, concerns for these vehicles include the release of CO₂ as well as a number of other environmental concerns.

At present, however, the best potential solution appears to be a fuel cell; PEM fuel cells in particular use hydrogen and produce no emissions (at the point of use).

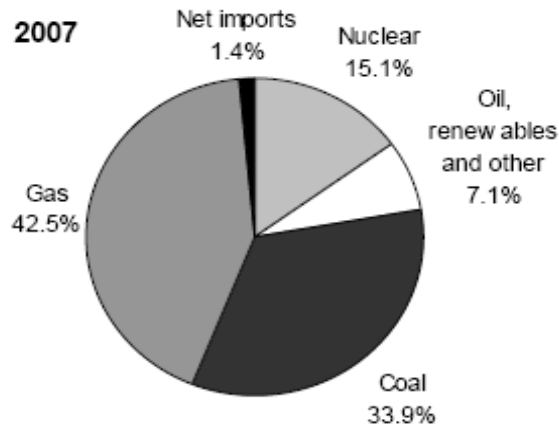


Figure 1 - Source of UK electricity generation in 2007³

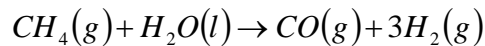
In the drive to reduce carbon emissions, and move away from our reliance on our depleting fossil fuels, hydrogen has been identified as a key alternative, due to its: abundance on earth in the form of water; high energy content per unit weight⁷; ability to produce energy using a fuel cell with only the release of environmentally benign water as a by-product. However, drawbacks still remain, including the need for economic techniques to produce hydrogen through the breakdown of hydrocarbons or the electrolysis of water, and the need for an effective storage method for use in mobile applications. Currently hydrogen is produced by a number of techniques including natural gas reformation, coal gasification, the burning of biomass and the electrolysis of water.

1.1 Hydrogen Production

1.1.1 Steam Methane Reforming (SMR)/Steam reforming of natural gas

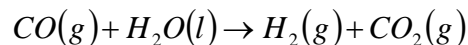
Steam methane reforming is currently the least expensive and most common method of hydrogen production, currently accounting for around 48% of hydrogen production globally. The process contains two steps, the reforming of natural gas (step 1) and the shift reaction (step 2) (equations 1 and 2). The second step occurs in two stages; stage one at the higher temperature of 350 °C and the second at the lower temperature of around 200 °C.

1. Reforming of natural gas



Equation 1

2. Shift reaction (water gas shift)



Equation 2

However, one major problem of this method is that the SMR process, carried out in large centralised plants, emits more than twice the amount of carbon dioxide than hydrogen produced.⁸ Production of hydrogen through steam methane reforming also leaves small amounts of carbon monoxide, carbon dioxide and hydrogen sulphide in the gas stream.

1.1.2 Hydrogen Production from coal (Coal Gasification)

Four different methods are commercially used in the process of gasification: counter current fixed bed gasifier; co-current fixed bed gasifier; fluidized bed reactor; and entrained flow

gasifier. Gasification is currently widely used for the production of electricity from fossil fuels.

Pulverized coal is generally used in fossil fuel power plants to produce electricity however, this method is 'dirty' and can operate with high pollutant loads. Gasification breaks down the coal into its basic chemical constituents, and it occurs by reacting the coal at high temperatures and pressures with a controlled amount of oxygen, to produce syngas, a mixture of hydrogen, carbon monoxide, carbon dioxide and small amounts of sulphur compounds, which must then be scrubbed and further purified to remove the pollutants. Currently available large supplies of coal in politically stable countries mean this method is being revisited as a possible valuable energy source. However, it is almost twice as expensive to produce hydrogen from coal as from natural gas due to the ratio of hydrogen to carbon produced.⁹ Coal gasification produces large amounts of carbon dioxide which must be captured and sequestered if this is to emerge as an acceptable method of hydrogen production.

1.1.3 Burning of Biomass

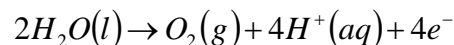
Biomass, the oldest utilized fuel, is sometimes described as carbon neutral because the absorption of carbon dioxide during photosynthesis equals that given off as it is burnt. Hydrogen is produced from biomass using either a process of pyrolysis or gasification. Both methods contain four similar steps, pre-treating, heating, 'scrubbing' (cleaning) and finally using the scrubbed gas to generate electricity. In pyrolysis, biomass is first ground into fine particles which are rapidly heated producing char, pyrolysis oil and syngas, which is used to produce electricity, unlike gasification, pyrolysis does not require oxygen.

1.1.4 Electrolysis of water

The electrolysis of water occurs by passing an electrical current through water which causes the decomposition of water into oxygen and hydrogen gas. An electrical power source is connected to two electrodes which are placed in the water; hydrogen appears at the cathode whilst oxygen appears at the anode. The addition of a catalyst such as a salt, or a base such as NaOH or KOH speeds up this process.

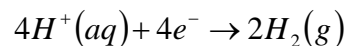
The process of electrolysis relies on controlling the voltage and current. Electrolysis of water usually begins at around 1.2 V and increases in rate as voltage is increased, typically being carried out at a voltage of 6 V.

Anode Reaction



Equation 3

Cathode Reaction



Equation 4

Using a renewable energy sources such as solar, hydro or wind power to produce the electricity required for electrolysis means hydrogen can be produced in an environmentally friendly method.

1.2 Hydrogen in Transport

1.2.1 Internal Combustion Engines (ICEs)

Internal combustion engines currently used in cars and many vehicles run predominantly off petrol or diesel, however internal combustion engines can be run off hydrogen. Future

possibilities exist for hydrogen to replace petrol and diesel to fuel ICEs. Hydrogen has regularly been used to power engines in rockets due to its high energy-to-weight ratio¹⁰. ICEs can be adapted to run on hydrogen over a wide range of fuel air mixtures.¹⁰

1.2.2 Fuel Cells

Fuel cells can be used to directly convert hydrogen into electrical energy. A large number of applications exist for fuel cells but vehicles are seen as a major opportunity. The basic concept of a fuel cell consists of an electrolyte sandwiched between two electrodes. A variety of types of fuel cell exist with the main difference being the type of electrolyte used. The electrolyte of the fuel cell affects the operating temperature range and the chemical reactions that take place.

1.2.2.1 Proton Exchange Membrane Fuel Cells

The schematic diagram of a Proton Exchange Membrane Fuel Cell (PEMFC) is shown in Figure 2¹¹. In vehicular applications a PEMFC has many advantages as the electrolyte in this type of fuel cell is a solid polymer poly-perfluorosulfonic acid. PEMFCs operate at temperatures between 50-100°C and have an efficiency between 53-58% in vehicular applications.¹² Advantages of this type of fuel cell include the low operating temperature, and reduced corrosion due to the solid electrolyte. Against this must be set the fact that the catalysts (platinum) used are expensive and highly sensitive to poisoning, making the need for an extremely pure supply of hydrogen vital to prevent the poisoning of the fuel cell system by contaminants.

Poisoning of the fuel cell catalyst and membrane occurs due to the presence of a number of waste components which are found in the feed gas stream. CO binds strongly to Pt resulting in a reduction of catalyst surface active sites available for hydrogen adsorption and oxidation.¹³ In comparison CO₂ has a less severe effect although conversion to CO can occur on a platinum catalyst which then may lead to poisoning. H₂S and other sulphur containing components have an irreversible poisoning effect on the catalyst. When operating optimally with a pure supply of hydrogen to the fuel cell only water and heat are emitted as waste products. Purity of the input hydrogen feed is probably the dominant factor in determining the efficient running of the fuel cell for many years without damage occurring.

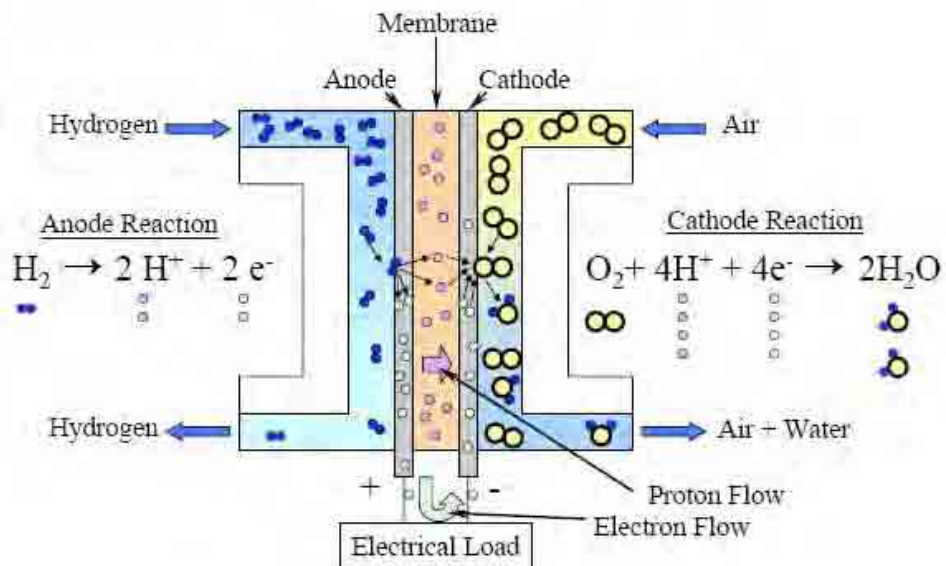


Figure 2 Schematic diagram of a PEM fuel cell¹¹

Operating experience has shown that even trace amounts of CO, CO₂, H₂S and NH₃ in the fuel stream can severely poison the fuel cell reducing performance¹³. This requirement for high purity hydrogen has led to the current upsurge in research into the development of suitable methods for hydrogen separation and purification. Currently hydrogen purification is carried

out through one of three main methods, pressure swing adsorption, microporous membranes and palladium-based membranes.

Whilst the technology currently exists to allow the purification of hydrogen, for the successful progression to an effective 'hydrogen economy,' further research is essential. Notably to: enhance hydrogen throughputs; and reduce costs. The main elements of current hydrogen purification technologies are reviewed in the following section.

2.0 LITERATURE REVIEW

2.1 Methods of hydrogen purification

2.1.1 Pressure Swing Adsorption

Pressure swing adsorption is a process that can be used to separate a required gas from a mixture of gases under pressure. Operating at near ambient temperature, adsorbent materials such as zeolites are used to sieve the gas mixture. At high pressures the impurities are selectively adsorbed onto the surface of the zeolite, leaving the purified hydrogen to be collected. The system then swings to low pressure to desorb the adsorbate. This method can produce high purity hydrogen of up to 99.999% v/v.¹⁴ Although this process can easily be scaled up it is hard to scale down and is not applicable for the purification of hydrogen on light vehicles, such as cars.

2.1.2 Porous Material Membranes

Porous materials such as ceramics, metals or polymers can be used as membranes for gas separation by the process of molecular sieving. Porous membranes are simple to operate, easily scaled down, reliable and cheap to run. Pore sizes can be tailored for a specific gas but < 1 nm is required for hydrogen¹⁵. Porous material membranes can be operated at higher temperatures than palladium based membranes and are not susceptible to hydrogen embrittlement or poisoning by H_2S ¹⁵. For fuel cell applications, a major limitation is that, hydrogen of only approximately 99% purity is produced¹⁵.

2.1.3 Palladium Based Membranes (Metal Membranes)

The purification of hydrogen through a palladium membrane produces purities of >99.9999% and also show high hydrogen recovery levels of up to 99% from hydrogen-rich gases.¹⁴ Hydrogen moves across a palladium membrane from an area of higher pressure to an area of lower pressure (Figure 3). On the up stream side of the membrane hydrogen mixed with other gases is present, hydrogen molecules are adsorbed onto the membrane surface, where they dissociate into hydrogen atoms. Ionisation of hydrogen atoms into hydrogen ions and electrons occurs on the membrane surface, before, diffusing through the bulk palladium membrane. On the down stream side of the membrane the re-association of H⁺ ions and the electrons occurs into hydrogen molecules occurs, followed by desorption of the hydrogen molecules away from the membrane surface.

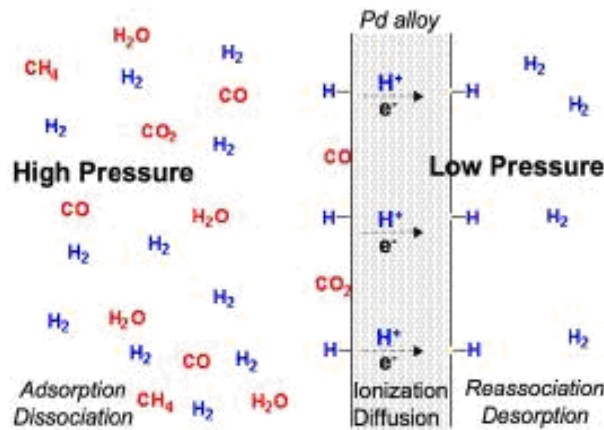


Figure 3 Schematic diagram showing the mechanism of hydrogen transfer across a metallic membrane¹⁶

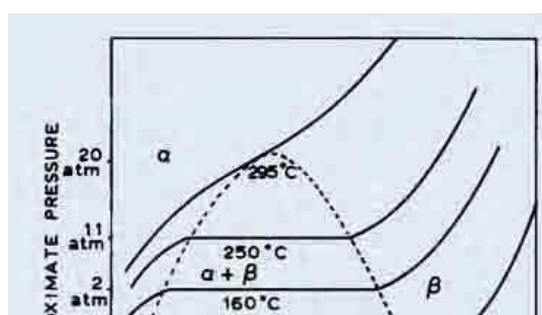
2.2 Metallic Membranes

Vanadium is one of the most hydrogen permeable metals due to its high hydrogen diffusivity and solubility,¹⁷ the intrinsic hydrogen permeability of vanadium, niobium and tantalum is much higher than that of palladium-silver.^{17, 18} However these materials have not been identified as suitable for hydrogen purification, due to hydrogen embrittlement problems especially at low temperatures.^{17, 18}

2.3 Palladium for hydrogen purification

Purification of hydrogen through metallic membranes has centred on palladium, due to its high selectivity, diffusivity and solubility for hydrogen. However, pure palladium has drawbacks. It is expensive (approaching 10 GBP per gramme¹⁹), and has a high susceptibility to poisoning by sulphur.²⁰ Difficulties may also be experienced when processing the palladium into thin defect-free membranes, as pure palladium has a Vickers hardness number of 47 (461 MPa).

Pure palladium has an f.c.c. crystal structure, the absorption of hydrogen into pure palladium causes the formation of two different f.c.c. crystal structures, with different lattice spacings. The phase transition ($\alpha \rightarrow \beta$) that palladium undergoes with increasing hydrogen concentration at temperatures below 300 °C (Figure 4) affects the materials properties; the β phase has a considerably expanded lattice compared to the α phase²¹ and so the existence of both the α and β hydride phases leads to warping and embrittlement²⁰ due to the co-existence of the two unequal f.c.c. phases of different unit sizes. Certain alloys of palladium do inhibit the $\alpha \rightarrow \beta$ transition and in use distortion is minimised, the overcoming of these problems is an area under much investigation.



The absorption of hydrogen into palladium causes two different f.c.c. phases to form: the alpha phase occurs at concentrations up to PdH_{0.02} whilst the beta phase occurs as hydrogen concentration continues to increase, and at hydrogen concentrations above PdH_{0.58} the alpha phase disappears (Figure 4).

2.3.1 Hydrogen Flux

Permeability of hydrogen through a metal membrane is a function of both hydrogen solubility of the membrane and hydrogen diffusion through the membrane due to the pressure difference that occurs between the upstream and downstream side of the membrane.

Sieverts' Law gives the concentration (c) of hydrogen on the metal's surface of the membrane

$$c = Kp^{0.5}$$

Equation 5

K is Sieverts' constant and p is the hydrogen pressure in the gas phase. From the application of Sieverts' Law it can be seen that at any given temperature the solubility of hydrogen in a Pd alloy should be proportional to the square root of the hydrogen pressure.

Hydrogen flux through a membrane is proportional to the difference of the square root of the hydrogen pressures on either side of the membrane and is calculated using Fick's Law.

$$J = \frac{\phi(P_i^n - P_{ii}^n)}{t}$$

Equation 6

J = Hydrogen flux

ϕ = Permeability

P_i = Up stream pressure

P_{ii} = Down stream pressure

t = Membrane thickness

In a bulk membrane n is given a value of 0.5 this value indicates that the rate limiting factor in hydrogen permeation through the membrane is the rate of diffusion of hydrogen through the bulk of the membrane rather than the other mechanisms, notably surface dissociation noted in Figure 3 where $n = 1.0$

The flux of hydrogen through a palladium membrane is therefore affected by a number of factors. An alloy with either increased hydrogen diffusivity or increased hydrogen solubility will give an increased flux. Hydrogen flux is also increased by increasing the area of the membrane, operating temperature and hydrogen differential pressure across the membrane. A decrease in the membranes thickness also leads to increase in flux. Decreasing the membrane thickness also allows for a lighter, less expensive membrane to be produced. However, a

stronger material or use of a membrane support maybe required for the thinner material to remain durable. In general, unsupported membranes are greater than or equal to 25 μm in thickness.

2.3.1.1 Guidelines and targets for a suitable hydrogen purification membrane²⁰

With the above mentioned factors in mind seven criteria have been set down for a practical hydrogen purification membrane material.²⁰

1. Minimal Palladium thickness (to reduce cost).
2. High permselectivity for hydrogen
3. High output per unit volume.
4. Steady and predictable performance over a long period of time at high temperature and pressure.
5. Adaptability to a variety of high temperature separation and membrane reactor applications.
6. Resistance to poisoning by hydrogen sulphide, chlorine, carbon monoxide and hydrocarbons.
7. Ability to with stand thermal cycling.

Taking these factors into consideration the US Department of Energy (US DoE) has set down a list of targets a practical membrane material should fulfil (Table 1).

Table 1 Targets set down by the US Department of Energy for a suitable material for hydrogen purification²²

Characteristics	Units	2003 status	DoE target
Flux Rate	Std. $\text{cc}/\text{cm}^2\cdot\text{min}$	30	100

	scfh/ft ²	60	200
Cost	\$/ft ²	150-200	<100
Durability	Hours	<1000	100000
Operating Temperature	°C	300-600	300-600
Parasitic Power	kWh/1,000 scfh	3.2	2.8

(Std.cc = standard cubic centimetres, scfh = standard cubic feet per hour)

At present there are no palladium based alloy materials capable of meeting all the US DoE targets.

2.3.2 Contamination and Poisoning

Contamination of palladium membrane surfaces is a serious performance limitation and results from one of three processes.²³

- i. *Segregation of bulk impurities at the surface* May occur due to impurities in the start material, which may gather on the surface of the membrane after annealing and so affect the interaction of hydrogen with the surface of the membrane.
- ii. *Formation of corrosion products prior to the interaction with hydrogen* May occur due to exposure to various elements, gases or liquids.
- iii. *Chemisorption of impurities in the hydrogen gas.* Whilst the aim of the palladium based membrane is to remove impurities from the hydrogen gas stream, certain sulphur and carbon-based impurities can lead to poisoning of the membrane.

2.3.2.1 Effect of Carbon Monoxide (CO)

The presence of CO in the gas stream can cause a decrease in the hydrogen permeation flux.²⁴ Reductions in the hydrogen permeation flux became more significant at lower temperatures or higher CO concentration.²⁴ Supplying H₂ and CO together at equal upstream pressures and temperatures below 150 °C rapidly leads to almost no hydrogen permeating the membrane. However, for temperatures above 300 °C, CO has almost no effect on hydrogen permeation²⁵ through palladium alloys. It would appear that the compounds limiting surface dissociation of hydrogen are desorbed above 300 °C.

2.3.2.2 Effect of Hydrogen Sulphide (H₂S)

The performance of palladium coated membranes can rapidly be destroyed after exposure to a H₂S containing gas stream and the poisoning effects maybe irreversible.²⁴ A rapid decline is also seen in hydrogen permeability of pure palladium membranes on exposure to H₂S.²⁶ For H₂S concentrations as low as 50 volume ppm in H₂, the flow rate of hydrogen through a 24 µm thick membrane at 350 °C with P1-P2 =170 kPa (1.7 bar) was reduced to about half its value for a clean surface in just 5 mins and about 20% of the clean value in about an hour.²⁷ The formation of pores²⁸ or cracks as palladium becomes palladium sulphide, which has a lattice constant twice that of pure palladium and leads to structural stresses on the surface may also occur allowing other gases to permeate through the membrane.²⁶ It was noted that the presence of H₂O along with H₂S increased the rate of sulphidation of the membrane.²⁸

2.3.3 Methods of Membrane Fabrication

A number of methods for the fabrication of membranes exist. Bulk membranes (25-100 μm) can be produced through a rolling process, whilst thinner membranes (5-25 μm) may be produced by sputtering, electro plating or electroless plating methods.

2.3.3.1 Rolling

Fabrication of bulk membranes is generally completed through the process of cold rolling. This method is suitable for production of high volumes of material. The process involves successively reducing the thickness of the material by passing the material through a pair of cold work rolls.

The process of cold rolling produces defects in the material, leading to an increase in strength and hardness whilst decreasing ductility hence increasing the risk of fracture. Intermediate annealing steps allow for ductility to be improved, allowing for further cold rolling to take place. Final defect densities in the membrane are closely correlated with the quality of the starting billet. The need to slowly reduce the material size and the possibility of intermediate anneals mean cold rolling can be a long process. Despite these limitations, Pd alloy membranes of several square centimetres with thicknesses of 5-10 μm have been produced by rolling.

Palladium has a preferential orientation in the (111) direction.²⁰ However this orientation is affected by the cold-rolling process for the fabrication of the membrane. Cold rolling causes disordering of the crystal structure (texture) of the material. The rolling process damages the crystalline order in the material and although annealing relieves some of the stresses produced in the material, new crystals that are produced during annealing have a different texture. The

degree of texture in a material depends on the number of crystals that have the preferred orientation. To observe the scatter about the ideal orientation can only be represented by means of a pole-figure which describes the spread of orientation about the ideal orientation for a particular set of poles.²⁹ Annealing of these materials usually causes formation of a new annealing texture.²⁹

2.3.3.2 Sputtering

Sputtering is a physical vapour deposition process commonly used for thin film deposition onto a substrate. The process occurs through the bombardment of a target by ions to eject atoms from the surface, which are then deposited on a support, forming a thin film. A number of sputtering techniques exist (including ion-beam sputtering, reactive sputtering, ion-assisted deposition, high-target-utilisation sputtering), in thin film membrane research when magnetron sputtering is used.

2.3.3.2.1 Magnetron sputtering

Magnetron sputtering is a process used to coat a substrate with a metal or alloy. The magnetron consists of a plate of the required coating (target) with magnets arranged behind this to create a magnetic trap for charged particles such as argon ions in front of the target. Turning on the power supply to the magnetron, puts the target at a negative voltage, which attracts argon ions to the target surface at speed, atoms are knocked out of the target surface, and when these atoms hit the sample surface a coating is formed.³⁰ This method can be used to produce thin films of varying thickness.

2.3.3.3 Electroplating

Plating gives layers of lower density than bulk materials. Incorporation of impurities in the film is very likely. Electroplating can be used to make a thin membrane by depositing a thin layer of metal onto a membrane support charged as a cathode. The process involves the use of an electrical current to reduce cations of palladium from a solution. The anode and cathode are attached to an external supply of current; the anode to the positive terminal and cathode (the item to be plated) is connected to the negative supply.

2.3.3.4 Electroless plating

Electroless plating is an autocatalytic process which occurs when the metal ion is reduced to a metal only on a specific surface, which must have a catalyst present before the reaction can begin.³¹

Electroless plating is the process of deposition without an applied current. It is possible for a limited number of materials and not suitable for all alloys. It is most commonly used for the plating of nickel, however, it is also commonly used in palladium membrane fabrication due to the ease and ability to produce good results. The process is a non-galvanic type plating method that involves several simultaneous reactions in an aqueous solution, which occur without the use of external electrical power.³²

2.4 Binary Palladium Alloys

In order to improve/eliminate the above stated issues of pure palladium (section 2.3), including the primary requirement of suppressing the α - β miscibility gap and therefore the distortion that is created, the alloying of palladium to form a number of binary alloys has been investigated.

Many palladium binary alloys have previously been explored, although the ones reviewed here have shown the best results for hydrogen permeability. Previous research has included Palladium-Silver^{21, 25, 33, 34, 35, 36, 37, 38, 39, 40} Palladium-Yttrium,^{21, 35, 38, 39, 40, 41, 42, 43, 44, 45} Palladium-Cerium,^{21, 39, 40, 41, 42, 43, 44} Palladium-Gold,^{21, 37} and Palladium-Copper^{21, 28, 46, 47, 48, 49, 50} alloys. For these alloys, improvements have been reported in: H₂ permeability; ability to withstand temperature cycling; resistance to poisoning; and strength.

2.4.1 Palladium Silver

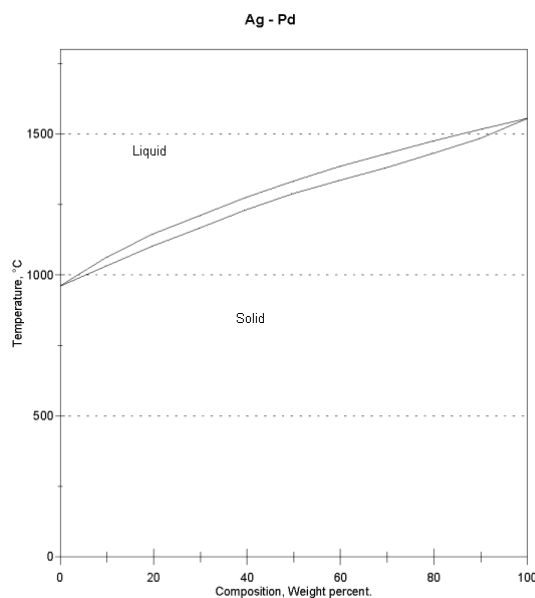


Figure 5 Phase diagram for palladium silver binary alloy⁵¹

Initial research on binary palladium alloys centred on palladium-silver, which is presently the main alloy used commercially for hydrogen purification processes. Extensive research into this alloy has shown that, although hydrogen diffusivity results for palladium silver show a reduction on those of pure palladium, this is compensated for by an increase in hydrogen solubility,²⁵ with an overall increase in hydrogen permeability. A complete range of solid solubility exist in the Pd-Ag system (Figure 5) but permeability in palladium-silver alloys

reaches a maximum in alloys containing 23-25at%Ag^{21, 35, 36}. Palladium-silver alloys also show increased strength compared to that of pure palladium. The hydrogen permeability of a Pd-25at%Ag alloy at varying temperatures and pressures is shown in Table 2. The hydrogen permeability of commercial Pd-25wt%Ag was not found to be affected by impurities such as NH, CH₄, CO, CO₂ and N, which are present in hydrogen at low concentrations (10 - 10000 ppm).³⁷

A further key feature of the alloying of palladium with silver is the avoidance of the α - β phase transition. Alloying palladium lowers the critical temperature for the α → β phase transition by narrowing the α / β -Pd hydride miscibility gap²⁰.

Table 2 Hydrogen permeability cm³/cm².sec of Pd-25at%Ag alloys at 200°C, 300°C and 400°C³⁸

	Pressure (atm)	200°C	300°C	400°C
Pd-25at%Ag	3.4 [3.4 bar]	0.133	0.075	
	6.8 [6.8 bar]	0.235	0.365	0.370

2.4.2 Palladium Yttrium

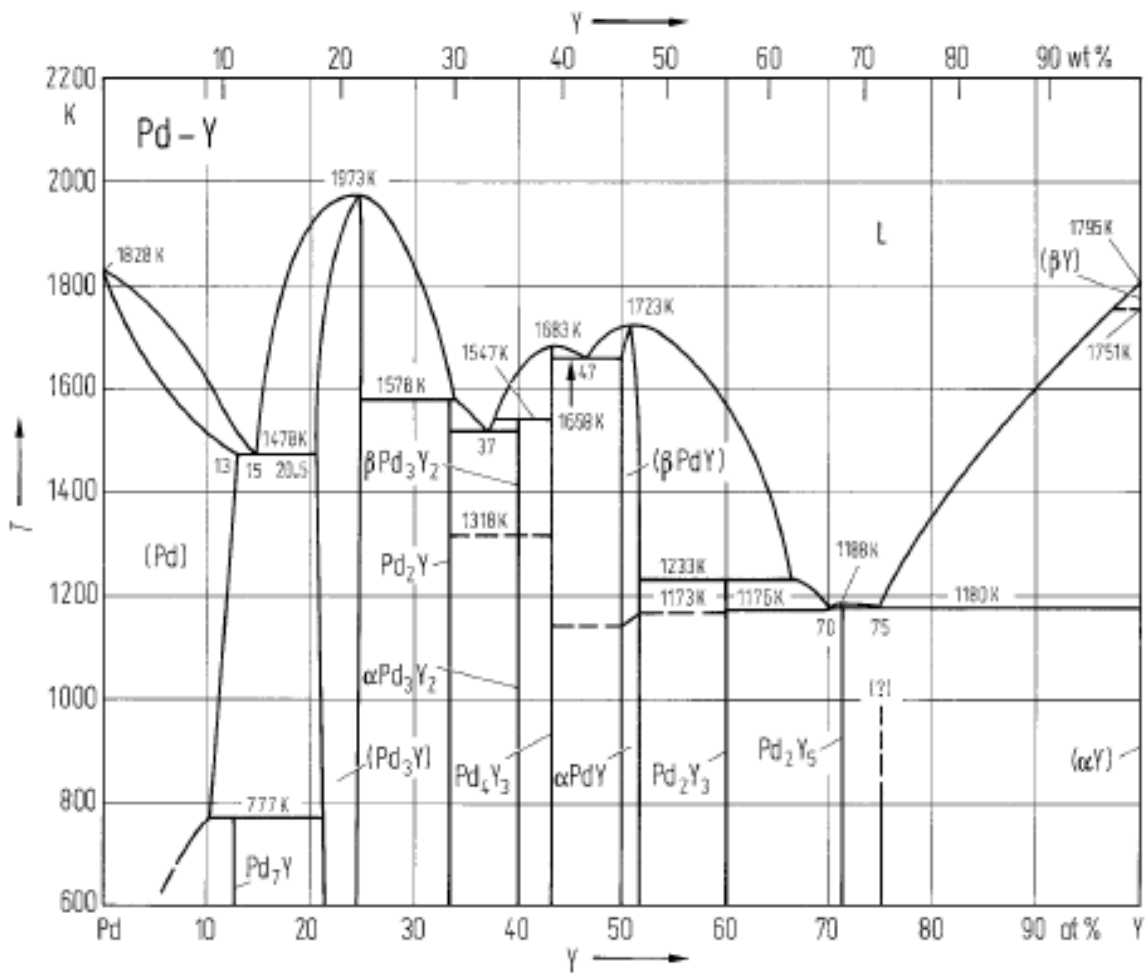


Figure 6 Palladium-Yttrium phase diagram⁵²

Yttrium is formally part of the Transition Group Metals although it is often referred to in palladium membrane research as belonging to the Rare Earth Group of Metals. This is due to its alloying behaviour which is similar to those of the heavy rare-earth metals. Previous workers research, have examined the result of alloying a number of rare-earth metals with palladium.^{39, 41, 42, 43} The solid solution alloys formed in the Pd-rich area of the Pd-Y system show the most promising results (Figure 6).

Research at Birmingham into the effects of alloying palladium with yttrium began in the 1960s and has explored the properties of alloys containing between 0 and 25 at%

Yttrium.^{35, 38, 40, 44} Room temperature x-ray diffraction data indicated that the α - β miscibility gap (see section 2.3) is closed at ~8 at% Y in the (Pd-Y)-H system³⁹ and alloys containing around 8 at% Y were shown to have the highest hydrogen permeabilities. The existence of a range of solid solubility for yttrium in palladium is not expected from the size-factor criterion of classical alloy theory.

2.4.2.1 Solid Solubility

The solid solubility of the alloy refers to the extent to which the alloying element will dissolve in the base metal, and according to the Hume-Rothery rules is related to crystal structure, atomic size, electronegativity, and valence.⁵³ The solid solubility of yttrium in the palladium-yttrium system, however, goes against the Hume-Rothery rule on atomic size which states that for solid solution to occur solute and solvent atoms must differ by no more than 15%, as the size difference of these two atoms is approximately 30%.⁴³ The solid solubility limit of yttrium in α -palladium is 12.2 at% Y at 900°C and 12 at% Y at 500°C.⁴¹ The relatively large solid solubility of palladium-yttrium is also present in a number of palladium-rare earth alloys and indicates the substantial proportion of the expansion of the α -palladium lattice by a solute atom has been attributed to the filling of the 4d electron states by the solute valence electrons.⁵⁴ A comparison of the effect on lattice spacings of palladium-silver and a number of palladium-rare earth solid solutions can be seen in Figure 7.

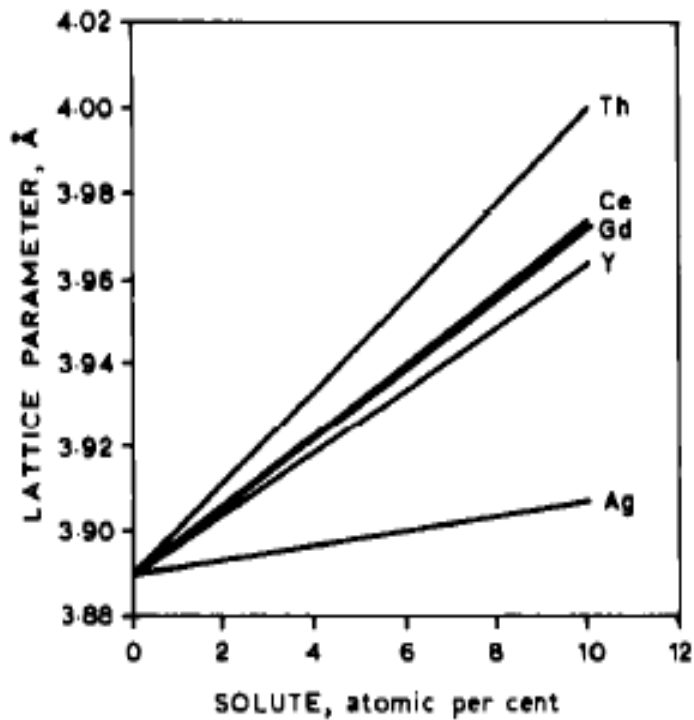


Figure 7 A comparison of room temperature lattice spacing of Pd-Ag and some palladium rare earth solid solution alloys with increasing solute concentration⁴³

2.4.1.2 Hardness and Strength

The addition of rare earths to palladium has been shown to lead to an increase in hardness as the rare earth content increases up to the solubility limit. This is to be expected given the large atomic size difference and hence associate lattice strain. Hydrogenation of the material reduces its hardness.⁴²

Fort et al.³⁸ anticipated appreciable solid solution hardening would be present in the Pd-Y alloys due to the large size difference between yttrium and palladium of 29% (compared to one of only 5% between palladium and silver in Pd-Ag alloys). In comparison to pure palladium and palladium-silver alloys, the alloying of palladium with yttrium creates a much

harder material. Hardness tests on Pd-Y alloys by Fort et al.³⁸ found Pd-8%Y to have a Vickers hardness number of 240 V.H.N in its annealed state compared to 90 V.H.N for a Pd-24at%Ag alloy, the hydrogenation of the Pd-Y alloy gives a reduction in hardness to ~180 V.H.N.

Whilst this increased hardness allows a stronger, thinner membrane to be produced, which can also withstand higher differential pressures across the membrane, it creates problems in the fabrication of a membrane when formed by the method of cold rolling. The membrane is more likely to become brittle and cracked due to the work hardening process. It is, however, possible to overcome this problem as the Pd-Y alloy becomes appreciably more workable after hydrogenation. Heating in a hydrogen atmosphere prior to rolling,^{35, 38} has been found to be beneficial and this process has been found to soften alloys with greater than ~3%Y content.³⁸ The cold rolling process causes work hardening to occur in the membrane as it is rolled. Internal stresses in the material can be reduced through intermediate annealing of the membrane as part of the rolling process.^{35, 38}

Wise et al.³⁹ found that the greatest hardening effect in the annealed material occurs when hydrogen content reaches the α_{\max} composition, whilst in cold rolled materials a distinct maximum in hardness occurs just before the on-set of the β phase.

2.4.2.3 Hydrogen Permeability

Investigation into the hydrogen permeability of Pd-8at%Y in comparison to those of Pd-25at%Ag and Pd-5.75at%Ce alloys at differential pressures of 3.4 and 6.8 atm (3.4 and 6.8 bar) over a temperature range of 20-500 °C has been carried out by Hughes and Harris.⁴⁰ The

results clearly indicate a much enhanced permeability of Pd-8at%Y (Table 3) at pressures of 3.4 and 6.8 atm (3.4 and 6.8 bar) and up to 400°C compared with that of Pd-25at%Ag (Table 2)³⁸ and Pd-5.75at%Ce, particularly at higher temperatures. (Figure 8 and Figure 9)

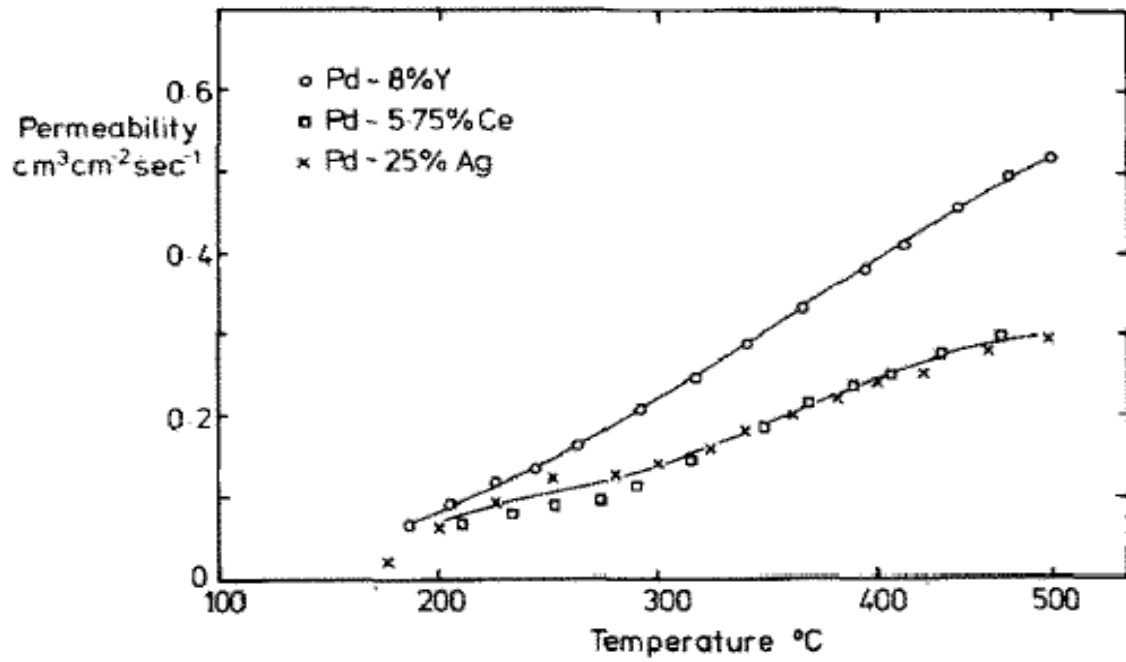


Figure 8 Comparison of permeabilities for Pd-25at%Ag, Pd-8at%Y and Pd-5.75at%Ce at 3.4atm⁴⁰

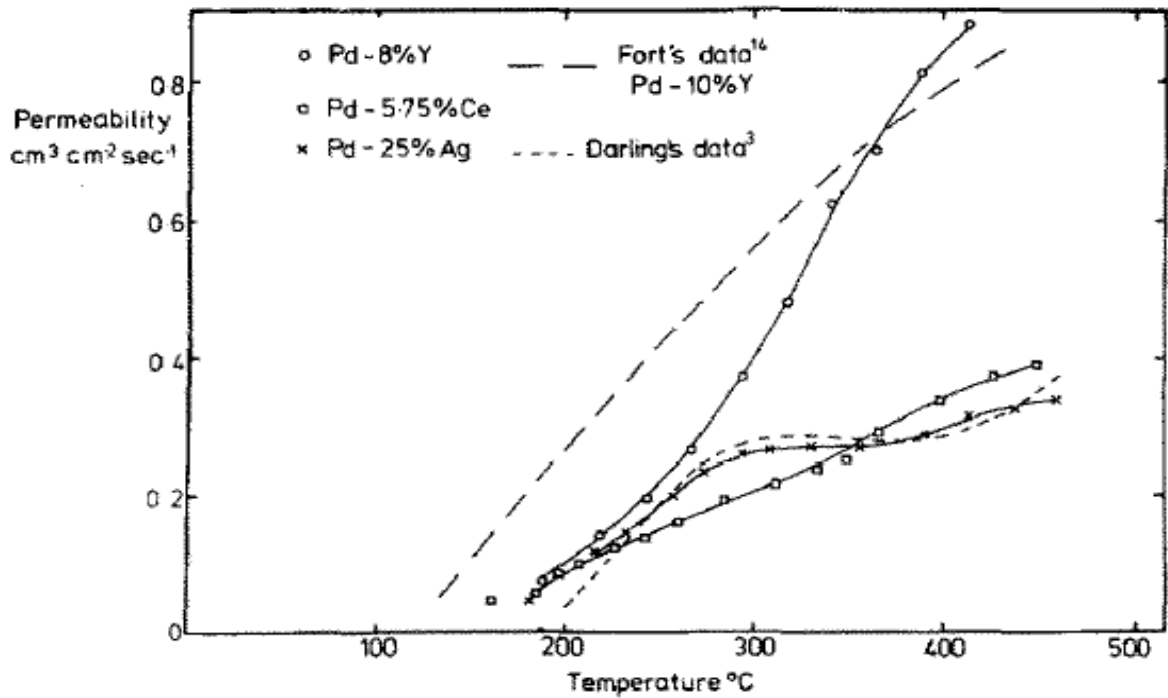


Figure 9 Comparison of permeabilities for Pd-25at% Ag, Pd-8at% Y and Pd-5.75at%Ce at 6.8atm⁴⁰

Hydrogen permeabilities from alloys with a Pd-6.6at% Y and Pd-10at% Y³⁸ at differential pressures of 10, 30, 50, 100 and 200 psi (0.6, 2.1, 3.4, 6.9, and 13.8 bar) and 293 and 673 K (20 and 400 °C) were clearly superior to those of commercial Pd-25at% Ag membranes.

Fort et al³⁸ identified a number of factors which influenced the permeability of hydrogen through a palladium based membrane and the reproducibility of permeability data recovered. These included:

- The previous treatment of the membrane. It was found that cooling in air or oxygen from above 600 K (327 °C), prior to a run, enhanced the subsequent permeability to hydrogen.

- The length of time at room temperature in air after a previous heating and cooling cycle. The membranes were found to poison in a comparatively short time if left in room temperature in air.
- The bleed rate. It was found that a bleed was only necessary if the hydrogen was very impure, or if the equipment was not properly evacuated prior to admitting hydrogen.

Table 3 Comparison of the hydrogen permeability $\text{cm}^3\text{cm}^{-2}\text{sec}^{-1}$ of Pd-Y alloys at 200°C, 300°C and 400°C

	Pressure (atm)	200 °C	300 °C	400 °C
Pd-6.6% Y	3.4 (3.4 bar)	0.188	0.113	0.063
	6.8 (6.8 bar)	0.325	0.65	0.69
Pd-8at% Y	3.4 (3.4 bar)	0.075	0.225	0.4
	6.8 (6.8 bar)	0.1	0.4	0.85
Pd-10% Y	3.4 (3.4 bar)	0.238	0.388	0.313
	6.8 (6.8 bar)	0.320	0.69	0.84

Further research into the permeability of palladium-yttrium alloys⁴⁰ showed this increase in permeability was due to the increase in the solubility of hydrogen in the membrane. Diffusivity of hydrogen in Pd-6at%Y to Pd-10at%Y show only a small variation with Y content.

2.4.2.4 Effect of Order

The large atomic mismatch in palladium-rare earth binary alloys makes them good candidates for short and long-range order. The strain energy associated with two widely different sized atoms can potentially be relieved by forming an ordered or partly ordered crystal structure.⁴¹

Hughes et al.⁴⁴ found Pd-8at%Y alloys to exhibit significantly enhanced permeabilities in the ordered condition compared with those of the disordered state. Their work also found, however, that the hydrogen solubilities of the material were not influenced significantly by the state of order of the alloy. Doyle and Harris⁴³ found hydrogen solubilities in palladium-rare earth alloys are affected by the order-disorder transformation, with disordered alloys absorbing more hydrogen than ordered alloys under identical conditions of temperature and pressure.

2.4.3 Palladium-Copper

More recent research has examined the benefits of alloying palladium with copper. One easily identifiable advantage of palladium copper alloys is the reduction in membrane fabrication cost by replacing costly palladium with much cheaper copper. Research has also shown some Pd-Cu alloys show improved hydrogen permeability, whilst others give improved resistance to poisoning by sulphur.

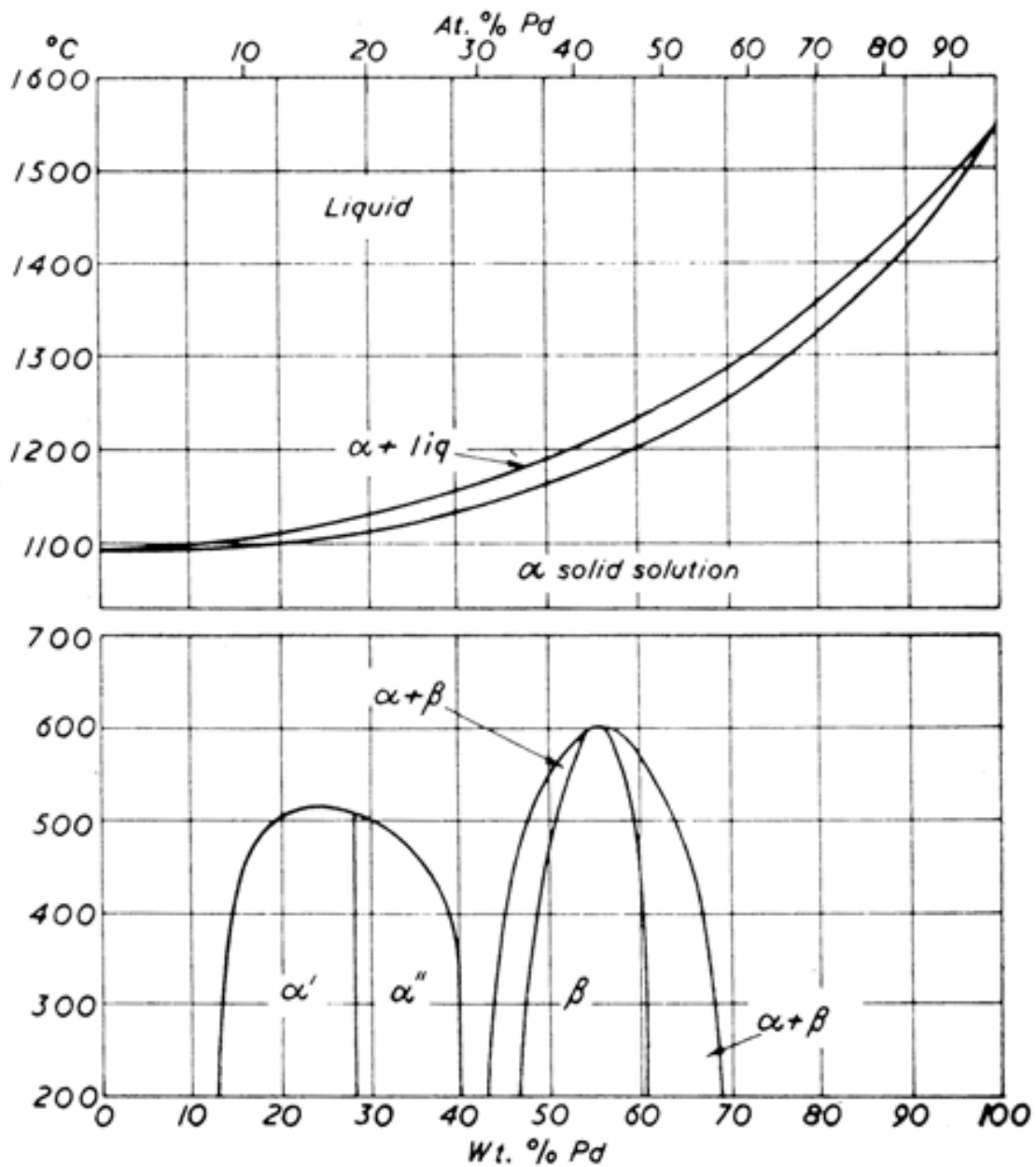


Figure 10 - PdCu phase diagram⁴⁸

2.4.3.1 The effect of crystal structure

The binary phase diagram for palladium-copper is shown in Figure 10. At high temperatures (760 °C) a complete range of solid solubility exists for Pd-Cu alloys, similar to the Pd-Ag system. At temperatures below 600 °C three ordered phases α' , α'' and β occur. The α' -phase has a face centre cubic crystal structure (f.c.c.), the α'' face centred tetragonal and the β -phase

is body centred cubic (b.c.c.). The copper content and the alloy and the alloy crystal structure (f.c.c. or b.c.c) affects both the hydrogen permeability of the membrane and the sulphur tolerance of the membrane. These effects will be further discussed in the two sections (2.4.3.2 and 2.4.3.3) below.

2.4.3.2 Hydrogen Permeability

Studies of the hydrogen permeability of palladium-copper alloys have found that permeability is a strong function of both alloy composition content and crystal structure.⁴⁶ McKinley⁴⁷ found that the permeability of palladium at 350°C decreases as additional amounts of copper are alloyed with palladium until approximately 30% copper, where the alloy has only 10% the permeability of pure palladium. However, as copper content increases to between 30 and 40wt%Cu, the permeability increases rapidly reaching a maximum at 40wt% Cu of around 1.5 times that of pure Pd at low pressures of 75 psig (5.2 barg) and between 1.25 and 1.5 times at higher pressures of 300 psig (20.7 barg) across the membrane. The alloying of additional amounts of copper (>40 wt%) sees a sharp decrease in permeability down to effectively 0 for alloys of composition Pd-60wt%Cu. In comparing these results to the crystal structure of the palladium-copper alloy it can be seen that hydrogen permeability increases in phase mixtures featuring the β crystal structure of the alloy and that maximum, permeabilities are seen when the alloy exhibits a completely β -b.c.c crystal structure. The hydrogen permeability of Pd-40wt%Cu is approximately 35% higher than that of pure Pd and almost 78% higher than that of Pd-5wt%Cu alloy.⁴⁸

A partial explanation for the higher permeability of a Pd-40wt%Cu alloy is due to the higher diffusivity of atomic hydrogen in the b.c.c (β - phase) crystal structure compared to that in the f.c.c (α -phase) crystal structure that occurs at lower Cu compositions.⁴⁸

2.4.3.3 Resistance to Sulphur

Whilst the alloying of copper with palladium may not enhance the levels of hydrogen permeability to those observed in palladium-yttrium alloys, the addition of copper leads to improved resistance of palladium copper to poisoning by sulphur.

It has been found that the concentration of H₂S in the hydrogen gas stream and not the time of exposure to the gas, was found to be the dominant factor leading to the failure of a both a pure palladium and a palladium-copper membrane²⁸ Hydrogen permeation was completely inhibited with a gas stream containing 100 ppm of H₂S in a palladium membrane, and 300 ppm in a Pd₆₀Cu₄₀ membrane.²⁸

The resistance of palladium copper to sulphur impurities in a hydrogen gas stream has been found only to exist in low copper content alloys with an f.c.c. crystal structure. In testing three Pd-Cu membranes, one from the b.c.c. (53wt%Pd) region, one f.c.c. (80wt%Pd) and one from the mixed b.c.c/f.c.c region (60wt%Pd) (border of the b.c.c, b.c.c. f.c.c mixed area) Rothenberg et al⁴⁶ found the 60wt%Pd alloy exhibited the highest permeability at temperatures up to ~500 °C but values dropped an order of magnitude as temperature increased and the alloy structure became f.c.c. The 80wt%Pd alloy showed permeability values of only 30% of those of pure Pd, but was not affected by the presence of H₂S in the gas stream.

As well as alloy composition, the membrane preparation technique has also been found to have an effect on Pd-Cu alloy membranes sensitivity to H₂S.²⁸ Cast and rolled foils have smoother surfaces and so present less surface area sites for the adsorption of sulphur, with less sulphur per unit area than rougher surfaces and so are less prone to surface modification by H₂S.²⁸

Despite the considerable amount of work devoted to the subject of sulphur poisoning of palladium-copper alloys, no definitive mechanism for the protective process offered by copper additions has been proposed.

2.5 Palladium Ternary and More Complex Alloys

2.5.1 Palladium-Yttrium (Gadolinium)-Silver

Previous work into ternary alloys has investigated the alloying of Pd_{100-x-y}Y_xAg_y and Pd_{100-x-y}Gd_xAg_y with varying silver concentrations (5-24at%Ag) and the condition of $y+3x \leq 24$.^{55,56} The X-ray studies of the annealed alloys showed that all the alloys form as a single α -phase, neither long range ordered compositions or intermetallic compounds were observed. In these alloys, maximum permeabilities were seen for compositions with 5at%Ag (y=5) and 6.3at%Y or 6.3at%Gd (x=6.3) and were 2-2.5 times higher than in the Pd-24at%Ag alloy.⁵⁶ These alloys also show greater hardness than for the Pd-24at%Ag alloy, although hardness is lower than for the Pd-8at%Y alloy.⁵⁵

2.5.2 Palladium-Yttrium-Indium (Tin, Lead)

Ternary alloys of Pd-Y-In(Sn, Pb) give improved hydrogen permeability over those of Pd-24at%Ag, in alloys measured up to 6at%Y. But permeabilities were not as high as the binary Pd-8at%Y alloy.⁵⁷ Over this range of compositions hardness tests have also been made

showing Pb additions gave a harder alloy than the Pd-Y binary and these alloys also showed the highest permeabilities of those tested.⁵⁷ Sn and In additions gave increased hardness at lower yttrium contents and slightly lower hardness above 2at% Y for In and above 4at% Y for Sn.⁵⁸

2.5.3 Palladium-Yttrium-Copper

A ternary alloy of palladium-yttrium-copper is of interest due to the properties of the Pd-Y and Pd-Cu binary alloys. There is, however, currently no published work on palladium-yttrium-copper alloys for hydrogen purification.

There are currently two different phase diagrams which have been produced for palladium-yttrium-copper.^{59 60} Figure 11 and Figure 12 show variations in the two diagrams exist especially in the Pd-rich Y-Cu region for which the samples that will be produced for this work fall.

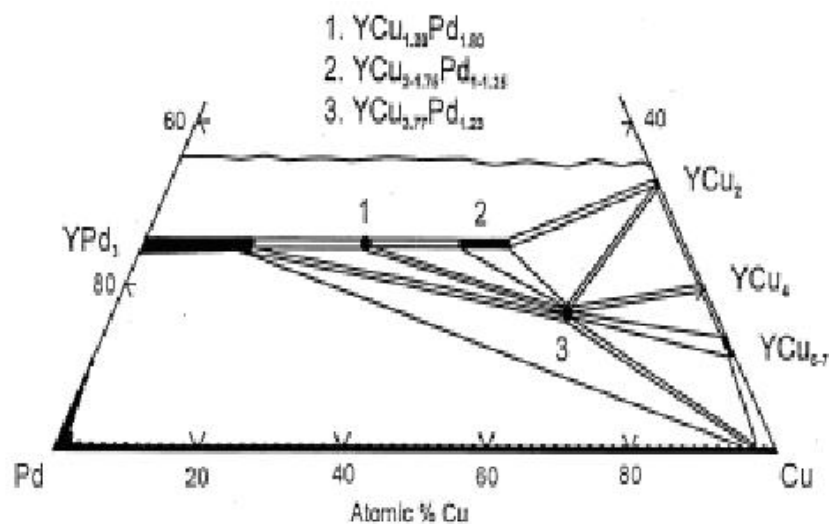


Figure 11 Palladium-Yttrium-Copper phase diagram at 600°C⁵⁹

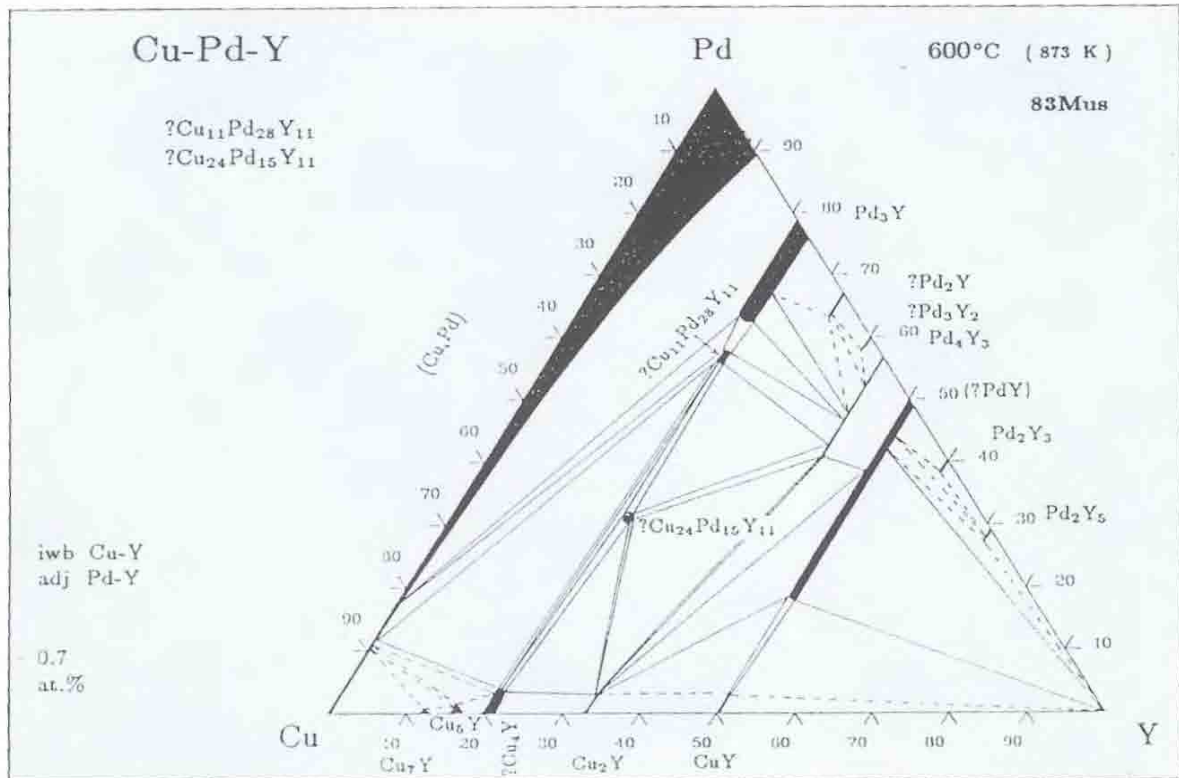


Figure 12 Ternary phase diagram for Pd-Y-Cu⁶⁰

2.6 Summary

In summary the presently commercially used palladium silver alloys for hydrogen purification exhibit improved hydrogen permeability and strength over pure palladium, exhibiting the best properties at 23-25at% Ag. The addition of yttrium to pure palladium enhanced permeabilities. The best alloy properties are at 8at% Y, which show higher permeabilities than Pd-(23-25)at.% Ag alloys. Pd-Y alloys are stronger and harder than Pd-Ag alloys, however, this can cause problems in membrane fabrication. The addition of copper to pure palladium also shows improvements in permeability over that of pure palladium, exhibiting a maximum at Pd-40at.% Cu, although these permeabilities are significantly below those of palladium-yttrium alloys. However, in contrast to Pd-Y and Pd-Ag, alloys this material has a b.c.c. crystal structure. A functional favourable feature of Pd-Cu alloy with an f.c.c structure

e.g. Pd-20wt%Cu is that this alloy exhibits resistance to poisoning by sulphur contamination, an important property for a hydrogen purification membrane.

The research into ternary alloys is limited although results combining palladium, silver and yttrium show that properties of the resulting alloys can be more favourable than the binary alloys. The most favourable Pd-Y-Ag alloys contain 5at%Ag and 6.3at%Y.⁵⁶

2.7 Aims and Objectives

Whilst the improvements in the hydrogen permeabilities of pure palladium by alloying with varying amounts of both yttrium and copper are well established, and the advantages of the ternary Pd-Y-Ag alloys have also been noted, there is currently no published work on ternary palladium-yttrium-copper alloys for hydrogen purification.

The aim of the current project is to combine results from previous research to prepare a number of Pd-Y-Cu alloys and through the process of cold rolling produce a bulk membrane with the f.c.c. crystal structure suitable for hydrogen separation and purification. The Pd-Y-Cu alloy membrane will be tested for hardness and ease of fabrication into membranes approximately 100 μm in thickness.

Scanning electron microscopy and X-ray diffraction will be used to investigate the membrane properties, and a hydrogen flow apparatus will be used to measure hydrogen flow and the effect of hydrogen sulphide on the membrane, hydrogen transmission properties. The results will be compared to those of binary Pd-Y and binary Pd-Cu alloys and most importantly, the Pd-Ag alloys with compositions typical of those used in commercial hydrogen purifiers.

3.0 EXPERIMENTAL

3.1 Sample Preparation

Calculations were made to determine the required amounts of palladium, yttrium and copper in atomic % to make samples with compositions Pd-8at%Y-10at%Cu, Pd-8at%Y-6at%Cu, Pd-8at%Y-3at%Cu, Pd-8at%Y-2at%Cu, Pd-8at%Y-1at%Cu and Pd-8at%Y-0.5at%Cu.

Palladium wire (99.95 % purity) was purchased from Umicore, yttrium (99.9 % purity) was purchased from Rare Earth Products, and copper wire (99.9+ % purity) was purchased from Sigma Aldrich. The required quantities to achieve the alloy composition were weighed, arc melted to form buttons, and then homogenised by heating in a vacuum at 950 °C for a week (as suggested in previous palladium, yttrium, copper ternary alloy work carried out in the lab⁶²). The homogenised buttons were cold rolled, wrapped in stainless steel foil, and vacuum annealed at 650 °C for four hours; the anneal is required to relieve the cold-working that occurs during the rolling process. This process was repeated until each approximately 4 g alloy button had reached a thickness of approximately 100 µm and finished with a final vacuum anneal.

3.2 Materials Characterisation

3.2.1 X-ray diffraction (XRD)

XRD was carried out on a Bruker D8Advance diffractometer using Cu K_α radiation (1.5406Å). Samples were mounted onto a sample holder and pressed flat before being loaded in to the machine. Measurements were taken from a starting (2θ) angle of 20° through to the end angle of 100°.

Lattice spacings for the Pd-Y-Cu alloys were derived from the observed 2θ reflections using Braggs Law

$$n\lambda = 2d \sin \theta$$

Equation 7

n = integer determined by the order given

λ = wavelength of the x-rays

d = spacing between the planes in the atomic lattice

θ = angle between the incidence ray and the scattering planes (Bragg angle)

All alloys observed in the present work had the f.c.c. crystal structure hence the lattice spacing a could be derived from the measured ' d ' value using

$$a = \frac{d}{\sqrt{h^2 + k^2 + l^2}}$$

Equation 8

a = lattice spacing

d = measured value from data

h, k, l = miller indices

Here, XRD lattice spacings of the material, identified the material's crystal structure, and showed the number of phases present in the sample. The method is non-destructive, allowing the same sample to be used for other analyses.

The analysis gained from XRD of thin films and membranes can also be used to note any rolling textures in material due to the method of production as a rolling texture affects the intensity of the peaks seen in the XRD trace.

3.2.2 Scanning electron microscopy (SEM)

Samples were mounted in Bakelite using a hot press, then ground using SiC paper with successively smaller grits down to 1200 grit before being polished with diamond paste to 1 μm , to ensure a smooth planar surface.

Scanning electron microscopy was carried out on a Jeol 6060 scanning electron microscope. Scans were taken in backscattered mode. Differences in image contrast allowed the identification of differences in structure that may have affected the fabrication and hydrogen flux through the material.

3.2.2.1 Energy Dispersive Spectrometer (EDS)

The SEM incorporates an INCA 300 energy dispersive spectrometer (EDS analyser) which allows for elemental analysis of the materials composition. This analysis was used to confirm whether the material is homogenised and whether the composition of the material corresponds to the 'as-weighed' target.

The system allows for point, zone, and line analysis, allowing for large areas to be analysed as well as specific points of interest. It is also possible to draw a line of points across the sample and so analysing a series of points with varying colour contrast that have been observed using the backscattered mode.

3.2.3 Hardness Measurements

Hardness measurements were carried out using a micro-Vickers hardness tester to compare samples in the 'as rolled' and 'as annealed' conditions. The anneal carried out before hardness testing was at 750 °C for 6 hours to allow results to be compared to previous work³⁸ on Pd-6.6at.%Y and Pd-10at.%Y alloys. Samples for hardness measurements were mounted as above before being ground and polished, to ensure they were completely flat.

The micro-Vickers hardness tester can apply loads of 10 g to 1 kg depending on the material and thickness of the sample. Due to the thinness of the prepared samples (40-100 µm) a 10 g load was applied with the diamond indenter the dimensions of the indent are then measured allowing the hardness tester to calculate the materials hardness.

3.2.4 Confocal Laser Microscope

The system allows for high resolution optical images of a sample to be created, and for 3D measurement of the sample topography to be captured, allowing the depth of any surface pores to be measured, and clearer images of how the surface changes across the sample to be viewed.

An Olympus LEXT confocal laser microscope was used to analyse the surface of the samples and note grain size and grain size distribution. The samples which had been previously used for hardness testing were viewed under the confocal microscope to analyse the depth and dimensions of the indents created. Samples were then etched using 30 % nitric acid, 70 % water, heated to 70 °C to allow clear images to be gained.

3.3 Materials Testing

3.3.1 Hydrogen Flow Rig

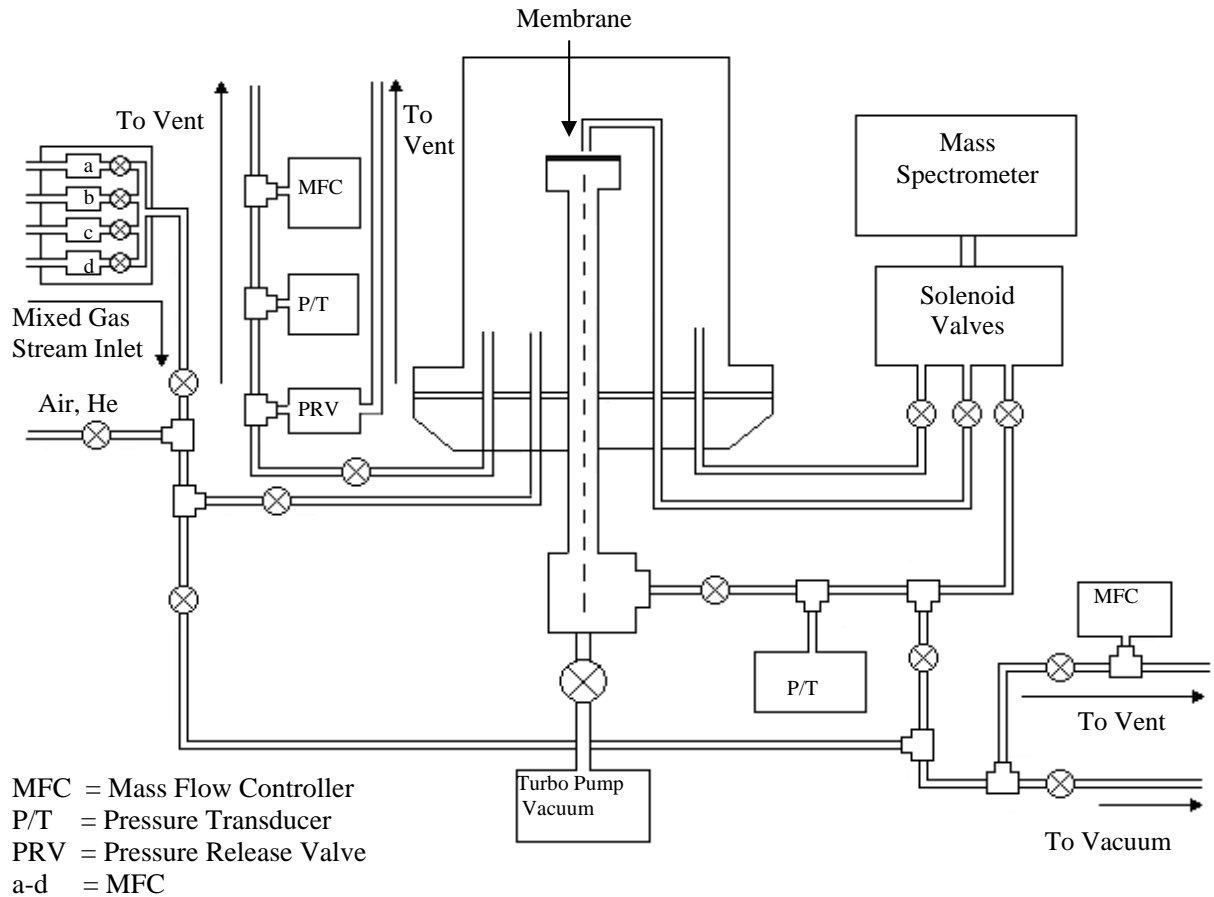


Figure 13 Schematic diagram showing the hydrogen flow rig⁶¹

The hydrogen flow rig (Figure 13) was constructed in the School of Metallurgy and Materials at the University of Birmingham, by Mr Sean Fletcher (PhD project). A schematic of the apparatus is shown in Figure 13. Hydrogen flux through a membrane can be measured and the design allows for the testing of the membrane when exposed to mixed gas streams as well as pure supplies of hydrogen.

The membrane is loaded into the chamber, using a copper gasket for support and pressed against a knife edge to gain a leak free seal. The chamber is then flushed through with helium to ensure all oxygen is removed from the system.

Hydrogen is then fed into the chamber and the membranes can be tested at varying temperatures and pressures. The upstream pressure was set at either 4.45 bara or 6.17 bara whilst downstream pressure is at 1 bar, giving a pressure variation across the membrane of 3.45 of 5.17 bar. The membrane can also be tested at temperatures varying from room temperature up to 500 °C. A typical temperature range in this work was 50-450 °C, with a pressure gradient of 3.45 bar.

Hydrogen passes through the membrane and is measured using a mass flow controller. A mass spectrometer is also connected allowing for a mixed gas stream to be analysed on the upstream side of the membrane, and for analysis of the gas which has passed through the membrane on the downstream side.

This piece of apparatus allows for hydrogen flow and hydrogen permeability through a membrane to be calculated. Hydrogen flow being the volume of gas diffusing through the membrane in a given time, whilst hydrogen permeability also takes into consideration the volume of gas passing through a unit area in a unit time per unit thickness.³⁸ Hydrogen flow rates need to be divided by membrane area and multiplied by membrane thickness to express the hydrogen permeability of the membrane.³⁸

4.0 RESULTS AND DISCUSSION

4.1 Initial Observations

The palladium-yttrium-copper alloy samples were cold rolled and annealed to produce films of approximately 100 μm in thickness. Previous work in the lab had suggested that small additions of copper made the alloys softer and that hydrogenation of the buttons would not be required for pre-roll softening, as is the case for Pd-Y alloys⁶².

Variations in hardness could be noted from the start of the rolling process in the Pd-8at%Y-3at%Cu, Pd-8at%Y-6at%Cu and Pd-8at%Y-10at%Cu samples. The Pd-8at%Y-3at%Cu alloy rolled easier and cracked less, and required fewer intermediate anneals to reach a thickness of 100 μm than had previously been found for a Pd-8at%Y binary alloy.

The addition of further amounts of copper (>3 at%), however, did not continue to increase the ductility of the material. Whilst it was possible to fabricate a membrane of 100 μm with the Pd-8at%Y-6at%Cu alloy with a number of additional intermediate anneals. The Pd-8at%Y-10at%Cu alloy was more brittle, showing crumbling and cracking, whilst rolling, even directly after annealing. It proved impossible to obtain a piece of material large enough to make a suitable test membrane.

Results from the initial alloys suggested only small amounts of copper were required to improve the ease of fabrication of the Pd-Y membranes. Further membranes were therefore fabricated with compositions of Pd-8at%Y-2at%Cu, Pd-8at%Y-1at%Cu and

Pd-8at%Y-0.5at%Cu. Of these membranes the Pd-8at%Y-0.5at%Cu rolled the easiest, requiring the fewest intermediate anneals of all the samples.

4.2 X-Ray Diffraction

XRD spectra were taken from the as-rolled foils to investigate the crystal structure, and identify any phases present. Clear peaks were observed on the Pd-8at%Y-3at%Cu (Figure 14) sample at 2θ values of 39.5° , 45.7° , 67° , 80.6° . Using *Equation 8* (Page 39) and the raw XRD data results indicate the alloy exhibits an f.c.c. crystal structure, with slightly larger lattice parameters than observed for the f.c.c. Pd-Y8at% parent alloy. The very large intensity of the 67° peak (220) suggests that rolling texture may have been induced, although further investigation of the effect of sample annealing on relative peak intensities is required to confirm this. Results for the alloys with lower copper concentrations Pd-8at%Y-2at%Cu (Figure 15), Pd-8at%Y-1at%Cu (Figure 16), and Pd-8at%Y-0.5at%Cu (Figure 17) were similar, showing peaks at 2θ values $\sim 39.4^\circ$, $\sim 45.6^\circ$, $\sim 66.8^\circ$ and $\sim 80.3^\circ$, indicating the existence of an f.c.c structure.

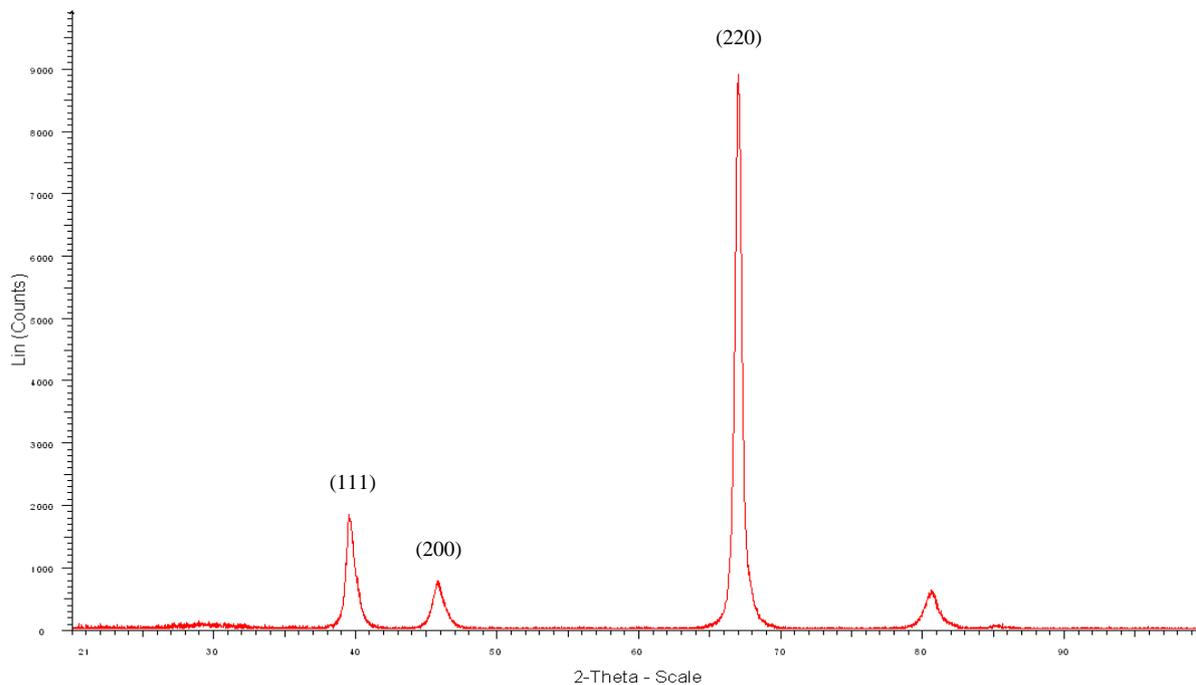


Figure 14 XRD trace Pd-8at%Y-3at%Cu

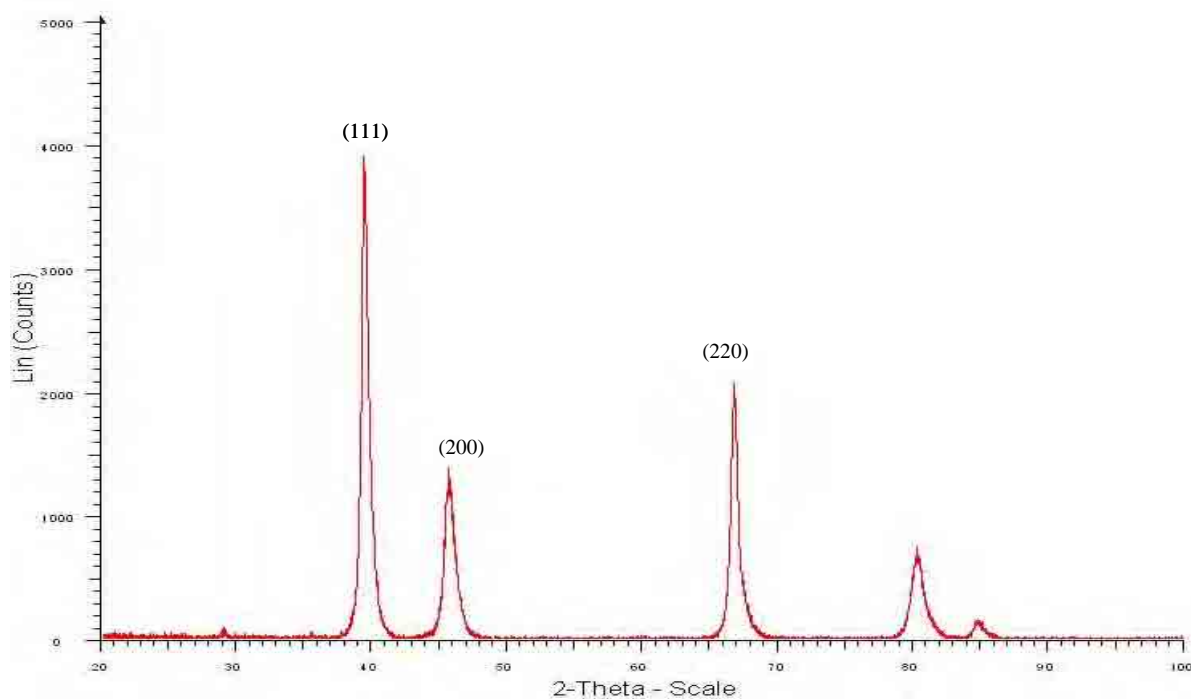


Figure 15 XRD trace Pd-8at%Y-2at%Cu

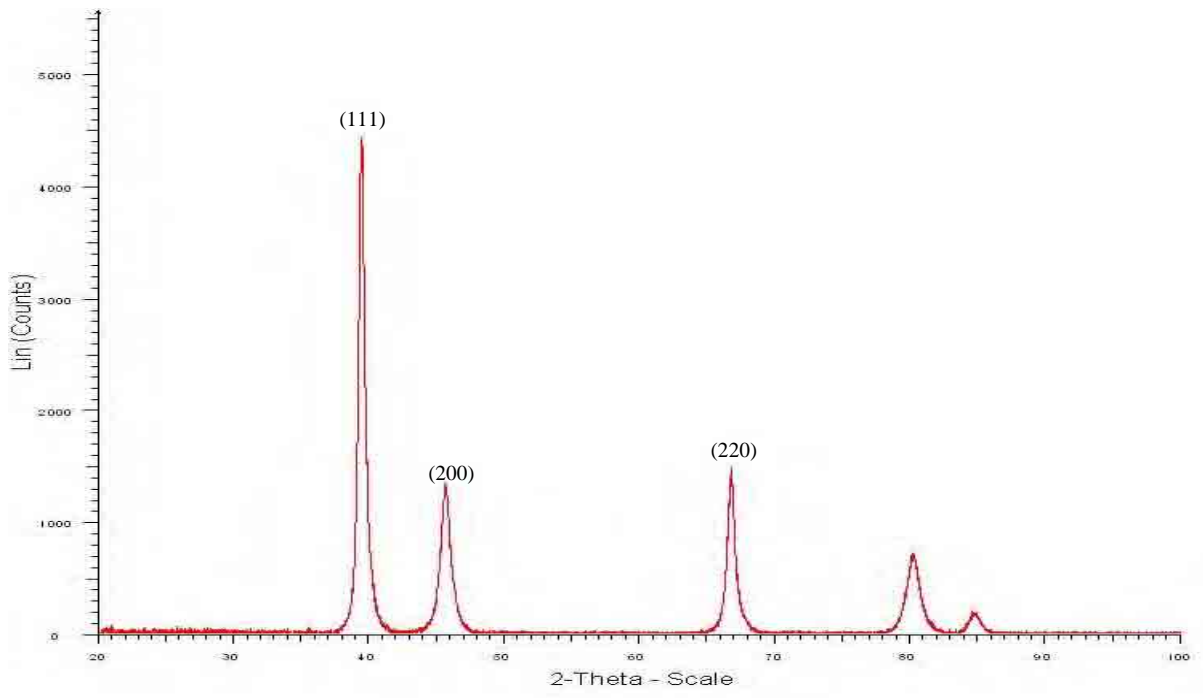


Figure 16 XRD trace for Pd-8at%Y-1at%Cu

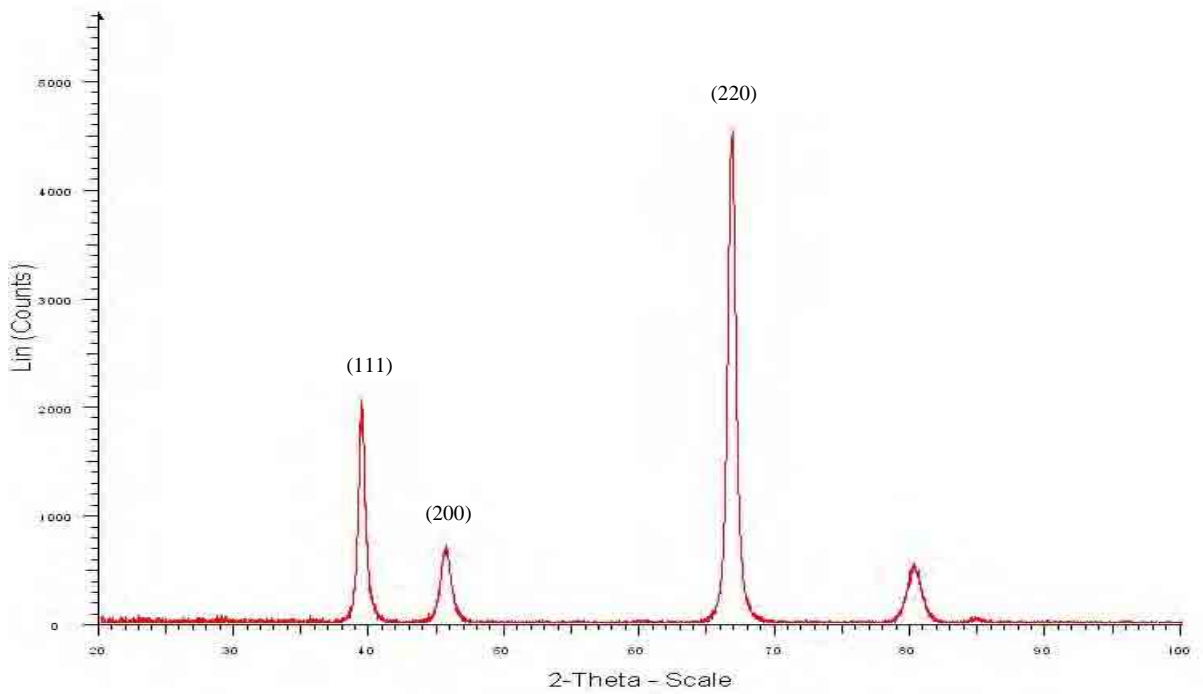


Figure 17 XRD trace for Pd-8at%Y-0.5at%Cu

However, XRD for the Pd-8at%Y-6at%Cu (Figure 18) alloy shows some peak splitting with peaks appearing at 2θ values of 38.3° , 40.1° , 46.6° , 64.9° , 67.1° . In the Pd-8at%Y-10at%Cu sample, the emergence of a further peak at 44.5° (Figure 19) suggest a second f.c.c. phase is forming.

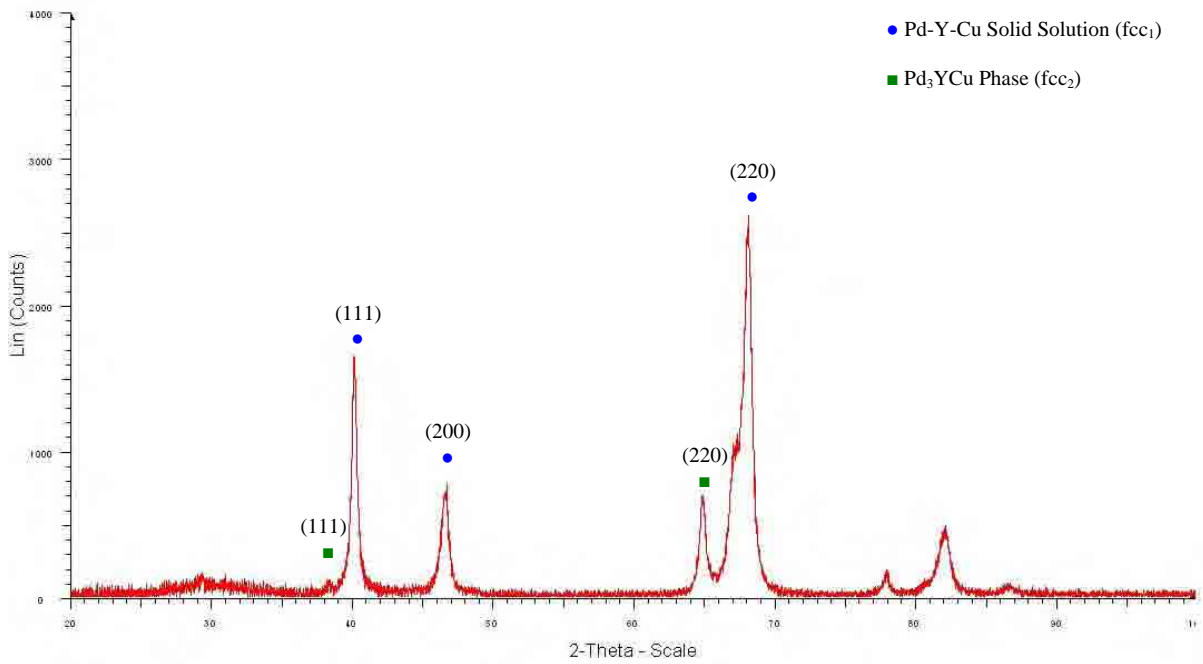


Figure 18 XRD trace Pd-8at%Y-6at%Cu

To establish the identification of the two apparent crystal structures visible in the XRD of the Pd-8at%Y-6at%Cu and Pd-8at%Y-10at%Cu alloys calculations of the two f.c.c. lattice spacings were carried out using the equation $a = d\sqrt{h^2 + k^2 + l^2}$ where d is the d -spacing given from the XRD raw data and a is the f.c.c. lattice spacing. The lattice spacings of the two f.c.c. phases are shown in Table 4 'a' should be equal for all f.c.c. peaks of the same structure.

Table 4 Calculated 'a' values for the Pd-8at%Y-10at%Cu alloy which suggest a second structure is forming.

2 theta (°)	a (Å)	
38.2	4.0701	fcc ₂ (111)
40.2	3.8794	fcc ₁ (111)
44.5	4.06148	fcc ₂ (200)
46.7	3.8865	fcc ₁ (200)
64.8	4.0624	fcc ₂ (220)
67.3	3.8758	fcc ₁ (220)

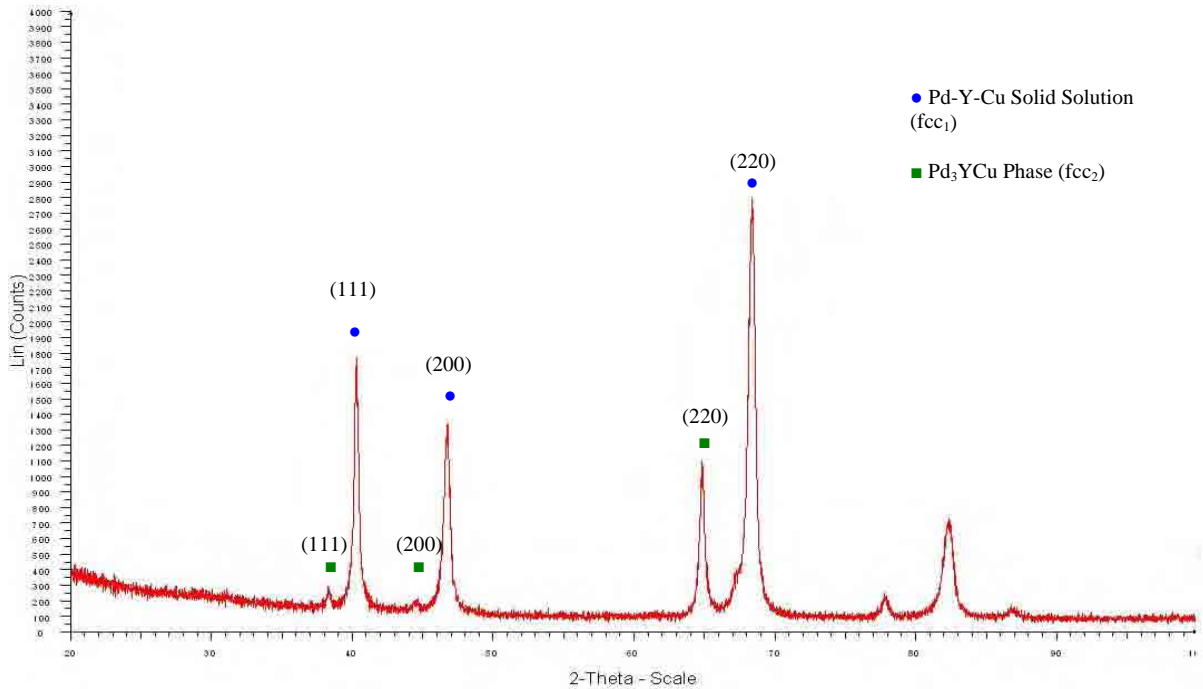


Figure 19 XRD trace for Pd-8at%Y-10at%Cu

The identified peaks can be linked to Pd-Y-Cu solid solution (f.c.c.₁) and Pd₃YCu phase (f.c.c.₂) and the lattice spacings are close to those reported by Kotur et al.⁵⁹ These peaks can be seen to be either side of the points at which the peaks occur in the binary Pd-8at%Y alloy which are identified in Table 5.

Table 5 Calculated 'a' values for the Pd-8at% Y alloy

2 theta (°)	a (Å)	
39.9	3.9292	(111)
46.1	3.9417	(200)
67	3.9508	(220)

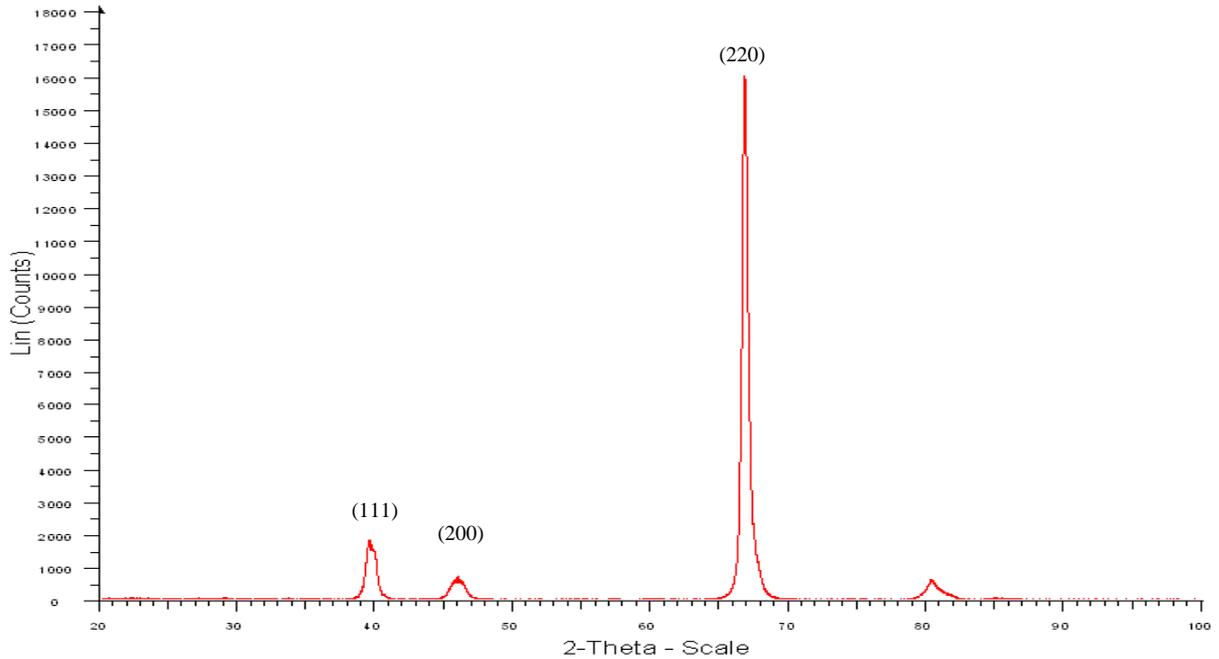


Figure 20 XRD trace Pd-8at% Y

XRD traces for the Pd-Y-Cu alloys shown in Figure 14 and Figure 17 exhibit strong 220 peaks related to other f.c.c. reflections. A feature which is also present in the binary Pd-8at% Y alloy (Figure 20).

The relative intensities of the peaks of a random (isotropic) sample and the disordered samples were compared (Table 6). Theoretical values for a completely random sample and measured values from our Pd-8at% Y-3at% Cu and Pd-8at% Y-10at% Cu were used. The results show the Pd-8at% Y-3at% Cu alloy in particular is strongly textured whereas the value for the Pd-8at% Y-10at% Cu and Pd-8at% Y-6at% Cu shows the texture is present but much weaker.

The Pd-8at%Y-2at%Cu and Pd-8at%Y-1at%Cu alloys show low texturing, whilst the Pd-8at%Y-0.5at%Cu texture is again signified.

In an XRD trace for a sample with a random structure such as that shown in Figure 21 which is an XRD trace for co-sputtered Pd-Y-Cu alloy film (additional work in the group)⁶³, it is expected that peaks will reduce in intensity as 2θ values increase.

The ideal intensities for 220/111 can be calculated and are listed in standard compilation such as the ASTM file. These are used in Table 6. The co-sputtered film also has a non-ideal texture, these are commonly observed in evaporated and sputtered films.

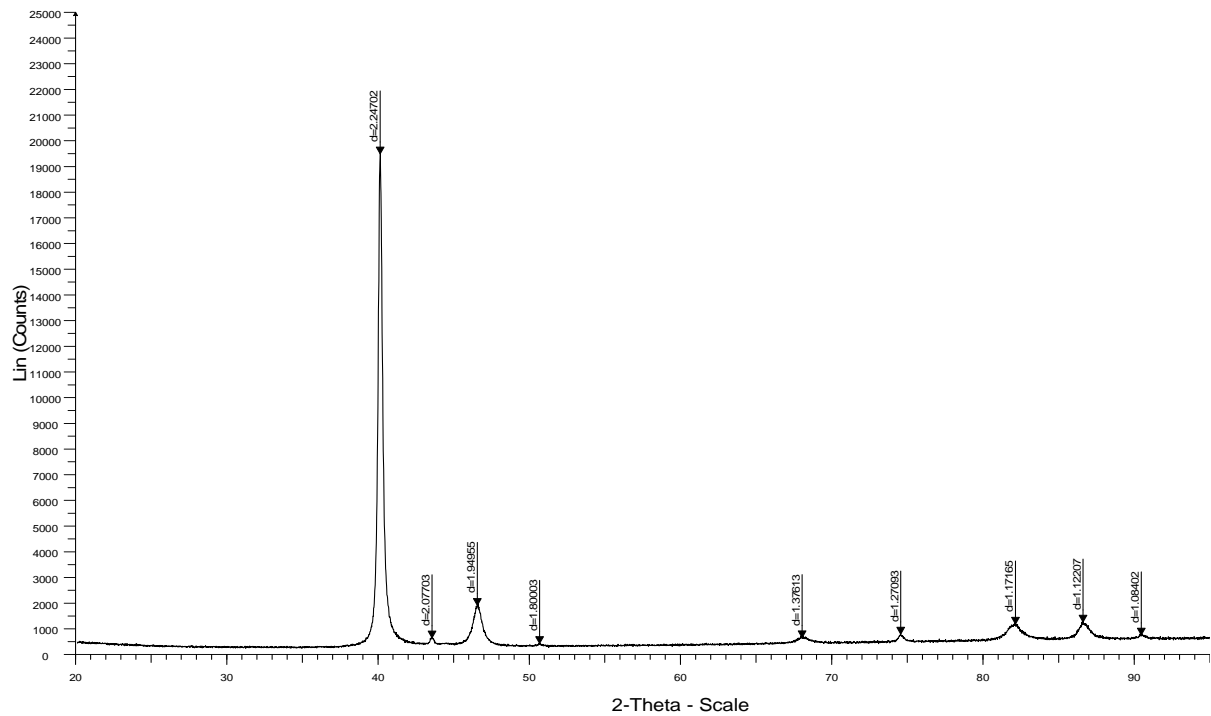


Figure 21 XRD trace for Pd-Y-Cu co-sputtered

Table 6 Relative intensities (220)/(111)

	Theoretical Value	Measured Values					
	Pd _{87.5} Y ₈ Cu _{4.5}	Pd ₈₂ Y ₈ Cu ₁₀	Pd ₈₆ Y ₈ Cu ₆	Pd ₈₉ Y ₈ Cu ₃	Pd ₉₀ Y ₈ Cu ₂	Pd ₉₁ Y ₈ Cu ₁	Pd _{91.5} Y ₈ Cu _{0.5}
Relative Intensity (220)/(111)	0.038	1.6	1.4	5.2	0.5	0.3	2.2

The f.c.c. lattice spacings of the Pd-8at% Y-3at% Cu, Pd-8at% Y-2at% Cu Pd-8at% Y-1at% Cu Pd-8at% Y-0.5at% Cu of all the alloys were calculated and are shown in Table 7. These values were then averaged and plotted as a function of composition and compared to published data for Pd-Y alloys and Pd-Cu alloys (Figure 22). Error bars were used for the Pd-Y-Cu alloys to represent the variation of the values to one standard error about the mean.

Table 7 Lattice spacings for some Pd-8at% Y-Cu alloys

	2 theta (°)		
	39.4	45.6	66.8
Pd-8at% Y-3at% Cu	3.9399 Å	3.9592 Å	3.947 Å
Pd-8at% Y-2at% Cu	3.9503 Å	3.9659 Å	3.9559 Å
Pd-8at% Y-1at% Cu	3.9586 Å	3.9753 Å	3.9579 Å
Pd-8at% Y-0.5at% Cu	3.9577 Å	3.9739 Å	3.9556 Å

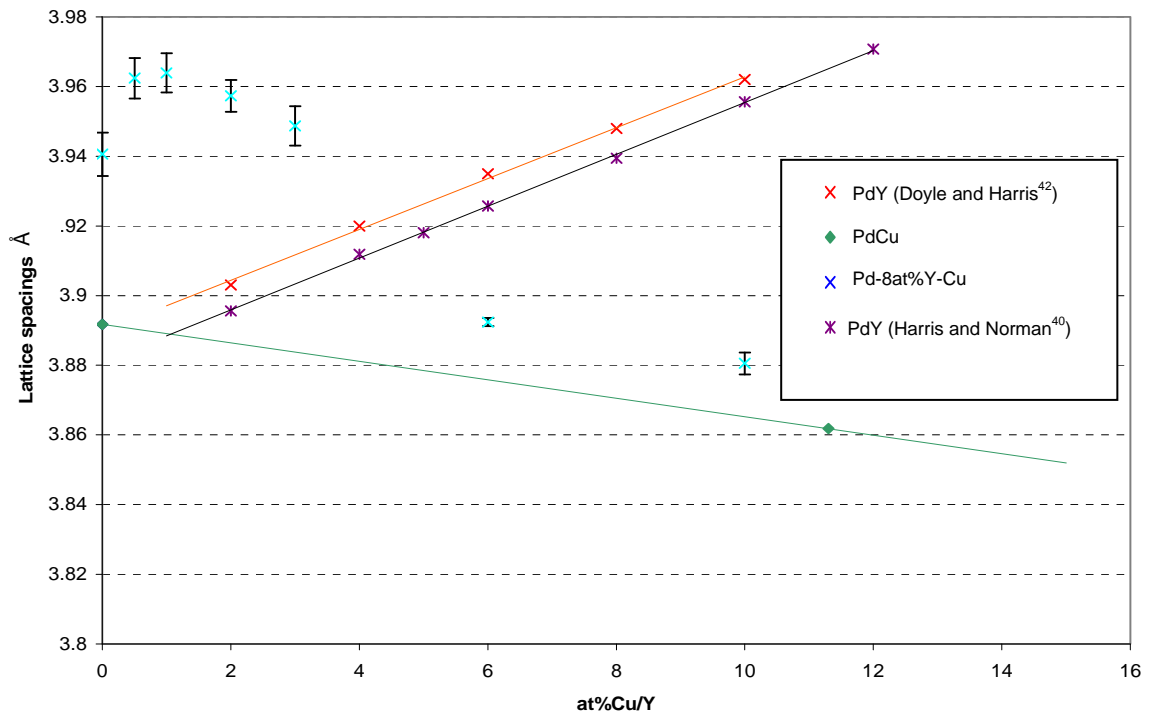


Figure 22 Lattice spacings for Pd alloys

From Figure 22 above it is clear that as the copper content increases in a Pd-Cu alloys, the lattice spacing decreases. This is due to the smaller atomic size of copper (1.35 Å) compared with that of pure palladium (1.4 Å). As might be expected the larger size of the yttrium atom (1.8 Å) increases the lattice spacing of the Pd-Y alloys as yttrium content increases. It should be noted that the lattice spacings of the Pd-Y alloys observed in the present work are very close to those of Harris and Norman⁴¹.

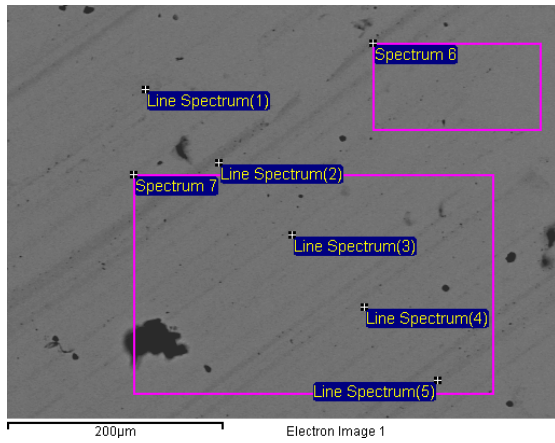
In contrast the linear expansion of Pd-Y lattice spacings have not been seen with the alloys in the Pd-8at%Y-Cu series that have been investigated in this work. Addition of copper to a Pd-8at%Y alloy, even in small amounts (0.5at%Cu), might have been expected to show a decrease in Pd-Y-Cu lattice spacing based on Pd-Cu systems (Figure 22) The Pd-8at%Y-0.5at%Cu alloy has an expanded lattice compared with that of the Pd-8at%Y

lattice. The addition of a further 0.5at%Cu to create the Pd-8at%Y-1at%Cu alloy expands the lattice further before the lattice is reduced by the continued introduction of copper to the alloy. The reason for this expansion of lattice spacing for copper compositions up to (1 %) is unclear.

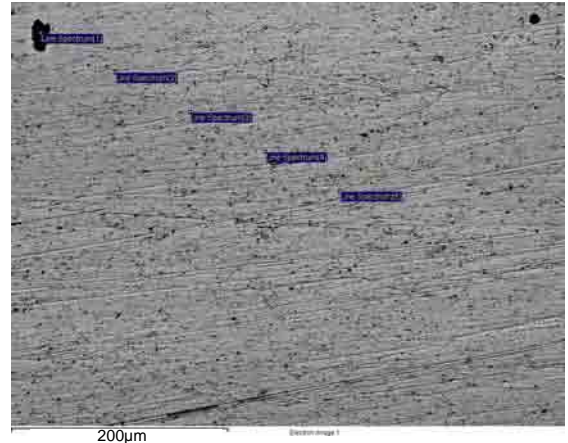
4.3 SEM AND EDS ANALYSIS

Backscattered images were taken of all Pd-Y-Cu alloy samples using the SEM (Figure 23-Figure 26). The images showed some regions of the sample were much darker than others suggesting the varying compositions across the sample, perhaps due to incomplete homogenisation.

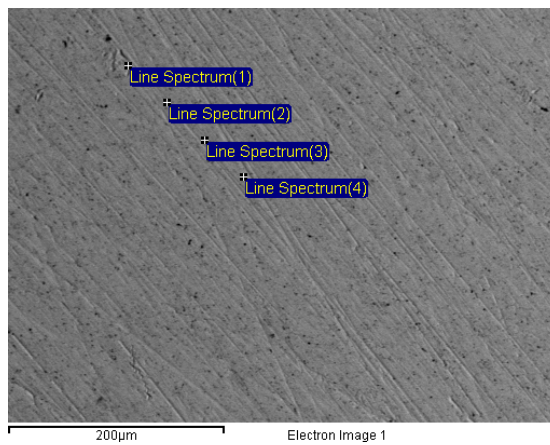
EDS analysis was used to investigate the degree of homogenisation of the samples, and any variation in composition. Both zone analysis (Figure 23a) and line analysis (Figure 23b) were used to compare large zones of the alloy which appeared uniform to spots and areas of varying colour which ran across it. These results were then compared and correlated to analyse the compositions of the samples (Table 8-Table 11).



a



b

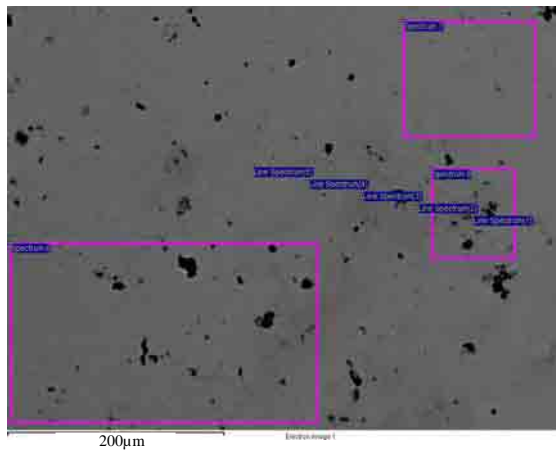


c

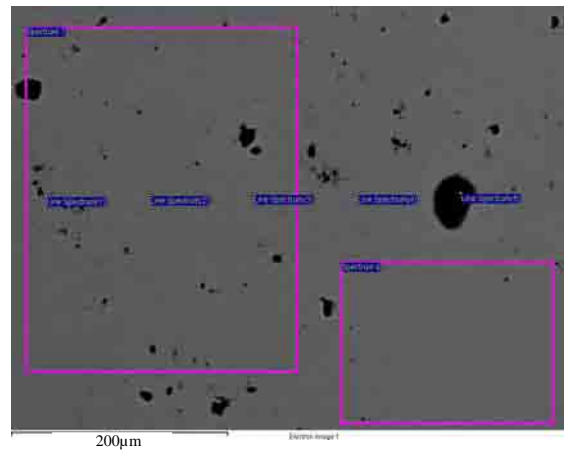
Figure 23 a, b, c SEM images taken during EDS analysis of Pd-8at% Y-3at% Cu

Table 8 Compositions of spectra for images Pd-8at%-3at% Cu (Figure 23)

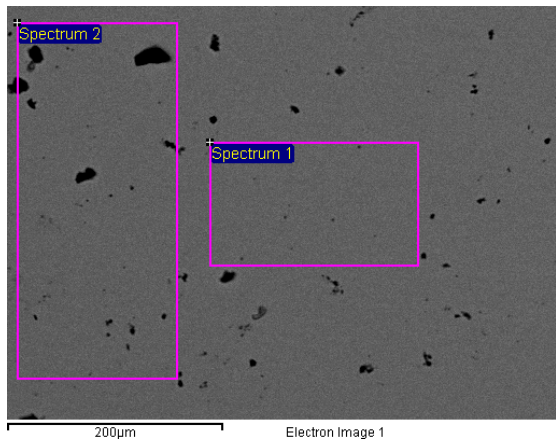
Image	Composition	Spectrum							Mean	Standard Deviation
		1	2	3	4	5	6	7		
a	Palladium	85.38	90.44	90.85	89.93	90.58	89.91	90.58	89.7	1.92
	Yttrium	10.11	6.78	6.26	6.77	6.5	6.72	6.4	7.1	1.35
	Copper	4.51	2.79	2.89	3.29	2.92	3.37	3.01	3.3	0.59
b	Palladium	89.93	89.42	91.37	89.55	90.09			90.1	0.78
	Yttrium	7.02	7.92	5.68	7.31	6.95			7	0.82
	Copper	3.05	2.66	2.95	3.14	2.96			3	0.18
c	Palladium	89.49	89.72	89.48	89.84				89.6	0.18
	Yttrium	7.3	7.36	7.61	7.09				7.3	0.21
	Copper	3.21	2.92	2.91	3.07				3	0.14



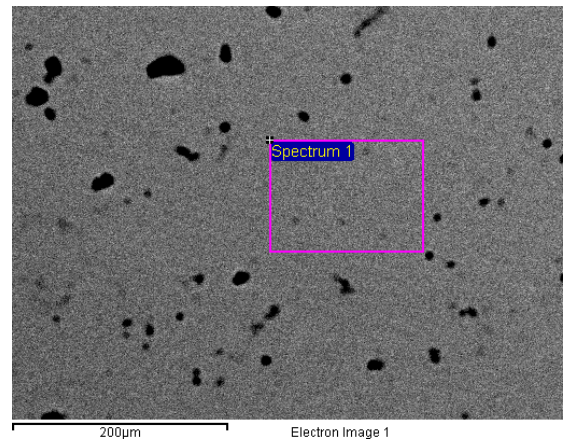
a



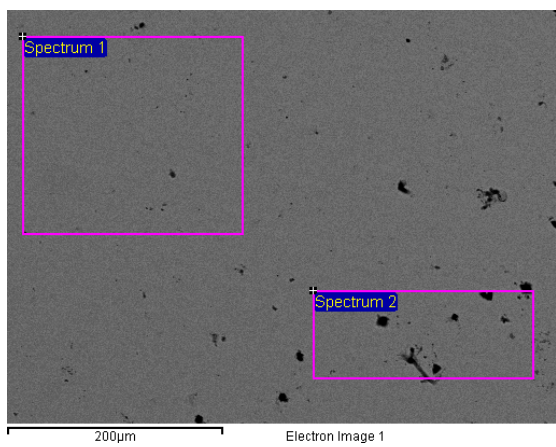
b



c



d

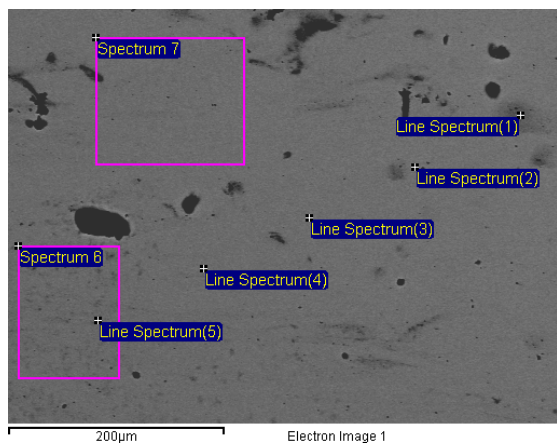


e

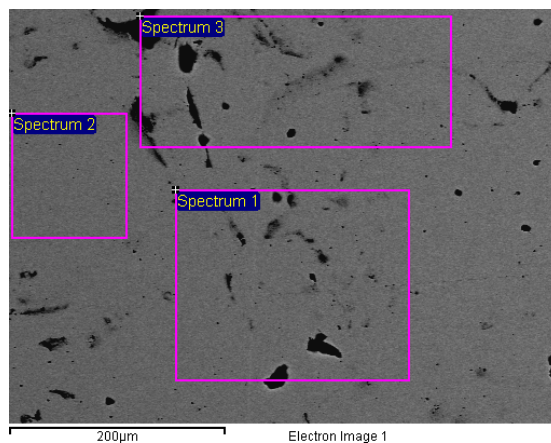
Figure 24 a, b, c, d, e SEM images used for EDS analysis Pd-8at% Y-2at%Cu

Table 9 Composition of spectra for images Pd-8at%Y-2at%Cu (Figure 24)

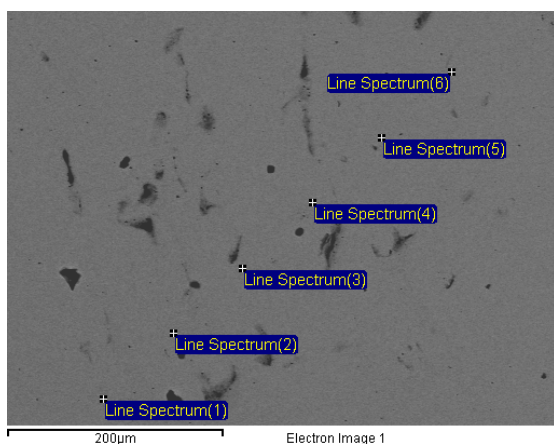
Image	Composition	Spectrum								Mean	Standard Deviation
		1	2	3	4	5	6	7	8		
a	Palladium	87.94	83.99	93.73	89.17	87.81	87.07	87.35	87.08	88	2.73
	Yttrium	9.13	14.51	2.76	8.53	10.46	10.35	10.15	10.92	9.6	3.29
	Copper	2.93	1.5	3.51	2.3	1.73	2.58	2.5	2.01	2.4	0.65
b	Palladium	89.04	88.83	88.98	88.53	93.44	89.59	88.9		89.6	1.72
	Yttrium	8.65	8.81	9.32	9.31	-0.01	8.22	9.2		7.6	3.4
	Copper	2.32	2.35	1.71	2.16	6.57	2.19	1.89		2.7	1.7
c	Palladium	88.6	88.84							88.7	0.17
	Yttrium	9.29	9.18							9.2	0.08
	Copper	2.11	1.98							2	0.09
d	Palladium	88.27								88.3	
	Yttrium	9.05								9.1	
	Copper	2.67								2.7	
e	Palladium	87.62	88.47							88	0.6
	Yttrium	10.21	9.13							9.7	0.76
	Copper	2.17	2.4							2.3	0.16



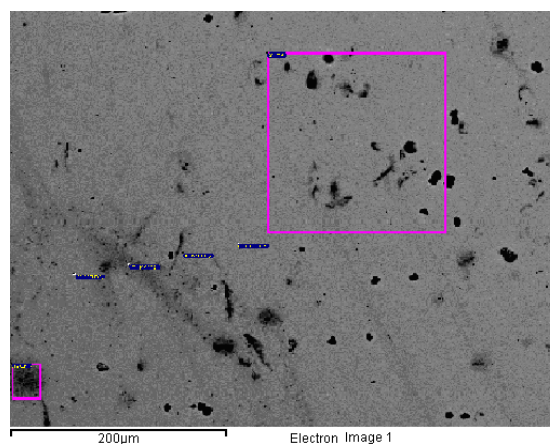
a



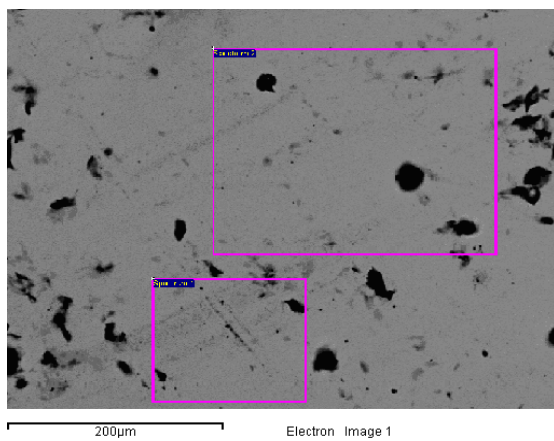
b



c



d



e

Figure 25 a, b, c, d, e EDS images for analysis of Pd-8at%Y-1at%Cu

Table 10 Summary of compositions for Pd-8at%-1at%Cu (Figure 25)

Image	Composition	Spectrum							Mean	Standard Deviation
		1	2	3	4	5	6	7		
a	Palladium	90.3	90.28	90.19	90.57	91.19	91.22	91.32	90.7	0.5
	Yttrium	8.56	8.42	8.72	8.25	7.8	7.68	7.77	8.2	0.42
	Copper	1.14	1.3	1.09	1.18	1	1.1	0.91	1.1	0.13
b	Palladium	90.95	91.52	91.15					91.2	0.29
	Yttrium	7.88	7.73	7.61					7.7	0.14
	Copper	1.17	0.74	1.24					1.1	0.27
c	Palladium	91.32	90.86	90.93	91	90.9	90.75		91	0.19
	Yttrium	7.74	8.06	7.84	7.9	8.15	8.02		8	0.15
	Copper	0.94	1.08	1.23	1.1	0.95	1.22		1.1	0.13
d	Palladium	91.13	91.05	91.57	91.04	91.27	90.89		91.2	0.24
	Yttrium	7.86	8.14	7.84	7.94	7.46	7.64		7.8	0.24
	Copper	1.01	0.81	0.59	1.02	1.27	1.47		1	0.31
e	Palladium	91.09	91.13						91.1	0.23
	Yttrium	8.37	7.95						8.2	0.3
	Copper	0.54	0.92						0.7	0.27

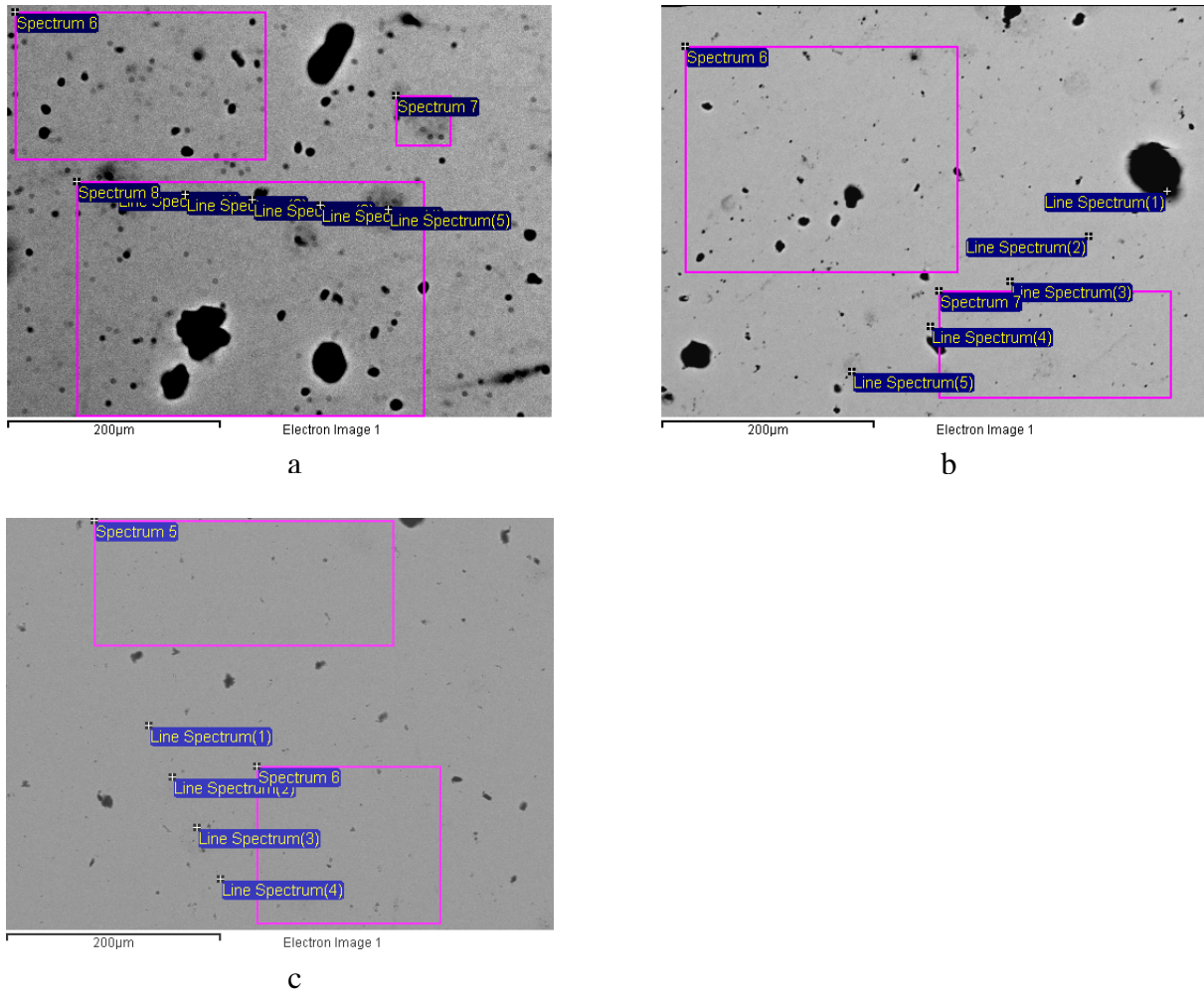


Figure 26 a, b, c SEM images used for EDS analysis of Pd-8at%Y-0.5at%Cu

Table 11 Summary of compositions for Pd-8at%Y-0.5at%Cu (Figure 26)

Image	Composition	Spectrum								Mean	Standard Deviation
		1	2	3	4	5	6	7	8		
a	Palladium	91.87	91.85	91.38	92.26	91.13	92.19	91.66	91.34	91.7	0.4
	Yttrium	7.55	7.94	7.83	7.43	8.2	7.64	7.91	8.24	7.8	0.29
	Copper	0.58	0.21	0.79	0.3	0.67	0.17	0.43	0.42	0.4	0.22
b	Palladium	90.92	91.76	91.63	91.36	91.84	91.5	91.8		91.5	0.32
	Yttrium	8.71	7.84	7.95	8.02	7.41	7.58	7.92		7.9	0.41
	Copper	0.37	0.41	0.41	0.62	0.75	0.92	0.28		0.5	0.23
c	Palladium	92.53	91.78	91.78	92.19	91.73	92.19			92	0.32
	Yttrium	7.37	7.58	8.22	7.7	7.38	7.76			7.7	0.31
	Copper	0.1	0.63	0.01	0.11	0.89	0.05			0.3	0.37

If the homogenisation step was completed successfully then samples should be consistent in composition (Table 8-Table 11). EDS measurements demonstrated that the samples were not completely homogenous, although taking averages across the samples in most cases gave composition close to those of the target compositions (Table 12)

The target gravimetric yttrium content of the four Pd-Y-Cu alloys was 8 at%, EDS analysis found some variation in these results for all the alloys (Figure 27). Data for the Pd-8at%Y-0.5at%Cu (Table 11) showed 80% of the results were within 6% of the 8 at%Y requirement. The same calculation for the Pd-8at%Y-1at%Cu alloys found 86% of measurements were within the 6% of 8at%Y target

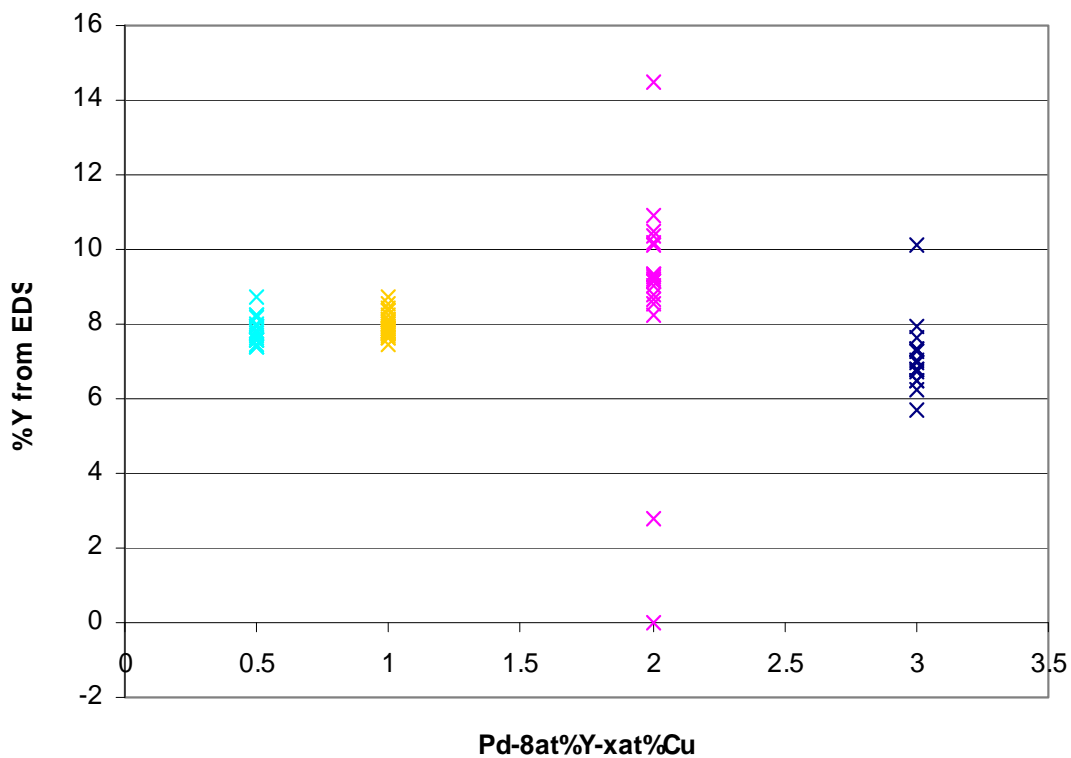


Figure 27 Percentage yttrium concentration as given from EDS analysis

The EDS analysis suggests the yttrium content of the alloy with the target composition Pd-8at%Y-2at%Cu (Table 9), is much higher with EDS measurements above 9 at%Y at most points in the alloy and above 10 at%Y at five points (Figure 27).

However in addition to the large number of points with higher measured yttrium content there were also a two of points measured in the sample showing very low yttrium contents, one area at 2.76at%Y and another where no yttrium was found. These results suggest incomplete homogenisation.

The degree of homogenisation in the Pd-8at%Y-3at%Cu alloy must also be questioned as the EDS analysis (Table 8) shows much lower yttrium content than the target composition of 8at%Y, with one area above having a yttrium content above 8 at%, whilst a number of points had yttrium contents below 7at%Y (Figure 27).

The copper content of the alloys also varies from the measured target value (Figure 28) in the Pd-8at%Y-0.5at%Cu alloy the copper content varies from as low as 0.01at%Cu up to 0.92at%Cu. For Pd-8at%Y-1at%Cu the variation is from 0.54at%Cu up to 1.47at%Cu. Copper content of the Pd-8at%Y-2at%Cu varies from 1.5-3.51at%Cu. The Pd-8at%Y-3at%Cu the variation in the copper content is from 2.66-4.51at%Cu.

Table 12 Summary of membrane composition

Target compositions	EDS measured composition %			Measured 'a' (Å)	Pd-8at%Y based 'a'(Å)
	Pd	Y	Cu		
Pd-8at%Y-0.5at%Cu	91.8	7.8	0.4	3.950	3.937
Pd-8at%Y-1at%Cu	91	8	1	3.957	3.94
Pd-8at%Y-2at%Cu	88.8	9	2.5	3.955	3.95
Pd-8at%Y-3at%Cu	89.6	7	3	3.945	3.93

The addition of Cu to Pd-Y-Cu alloys, by substitution of Pd, should lead to a reduction in the lattice spacing of the Pd-Y-Cu solid solution relative to that of Pd-8at%Y, as the atomic diameter of Cu (1.35 Å) is considerably less than that of Pd (1.4 Å). Even allowing for some scatter in composition across the membrane, all the lattice spacings show an increase over that expected by normal substitutional alloying in the absence of electronic or other factors affecting the lattice spacing Table 12.

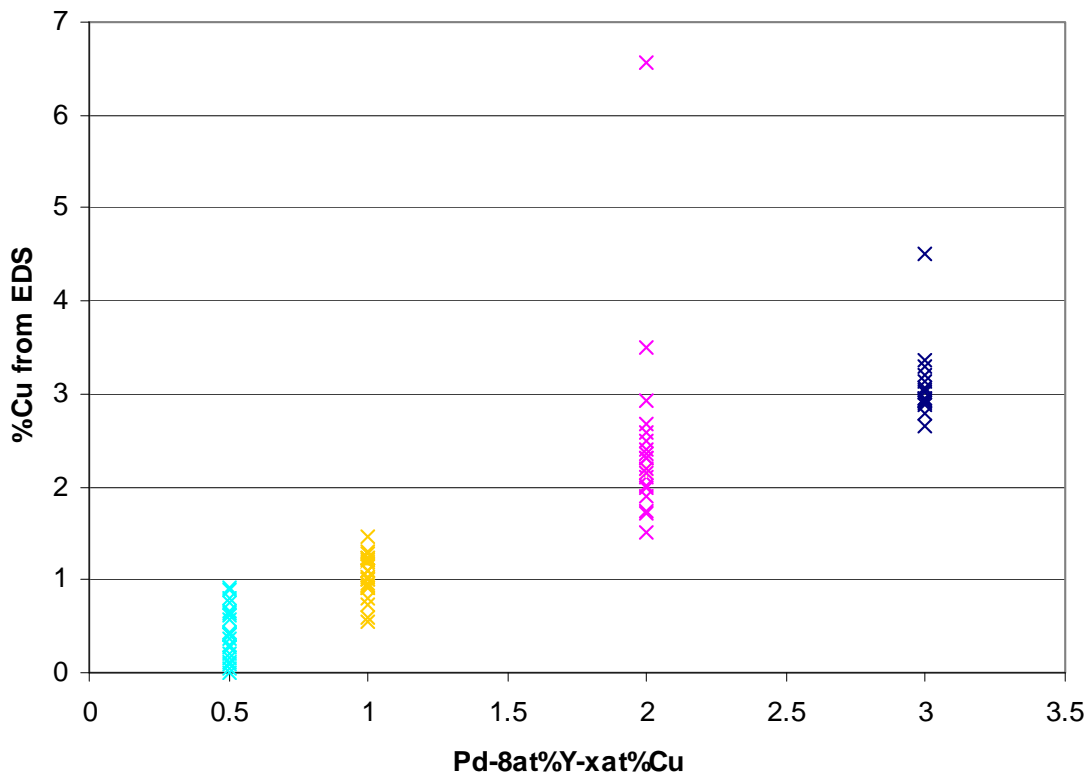


Figure 28 Percentage copper concentration as given from EDS analysis (Table 8-Table 11)

Given the variation in gravimetric measurement and EDS analysis, the exact nature of the variation with composition may not be as shown in Figure 22. However it is clear that the ‘a’ spacings variation is far from ideal.

The varying yttrium and copper contents of the four alloys in the Pd-8at%Y-Cu series show that the homogenisation of the samples was not complete. The variations in composition across the sample in both yttrium and copper content were much larger in the Pd-8at%Y-2at%Cu and Pd-8at%Y-3at%Cu alloys which showed areas of both high and low yttrium content, compared to the measurements on the Pd-8at%Y-0.5at%Cu and Pd-8at%Y-1at%Cu alloys which were more consistent in spread across the material. This is probably a contributory factor in the anomalous 'a' spacings seen in Table 12 and Figure 22.

4.4 MATERIALS HARDNESS

As discussed above, (Section 2.4.1.2) previous research has found Pd-8at%Y alloys to be considerably harder to roll than both Pd-Ag and Pd-Cu alloys. Hydrogenation was required to improve the ease of rolling^{35, 38}. In contrast, a Pd-40wt%Cu alloy has been found to be much softer and easier to fabricate into rolled membranes.⁶²

From initial observations whilst preparing the membranes in the Pd-8at%Y-Cu series through rolling, it was found that, generally, as the copper content increased the membrane became harder to roll. But further analysis of this general observation is required.

Hardness measurements were carried out on Pd-23at%Ag, Pd-40at%Cu, Pd-8at%Y, Pd-8at%Y-0.5at%Cu, Pd-8at%Y-1at%Cu, Pd-8at%Y-2at%Cu, Pd-8at%Y-3at%Cu materials. Initially, four results were taken for each of the above samples, although further tests were made on the Pd-Y-Cu series as results varied considerably. Some variations in hardness across the material maybe linked to the variations in composition shown across the material as

revealed by the EDS analysis. Variations are also likely to occur due to the variation in thickness across the material and the flatness of the surface.

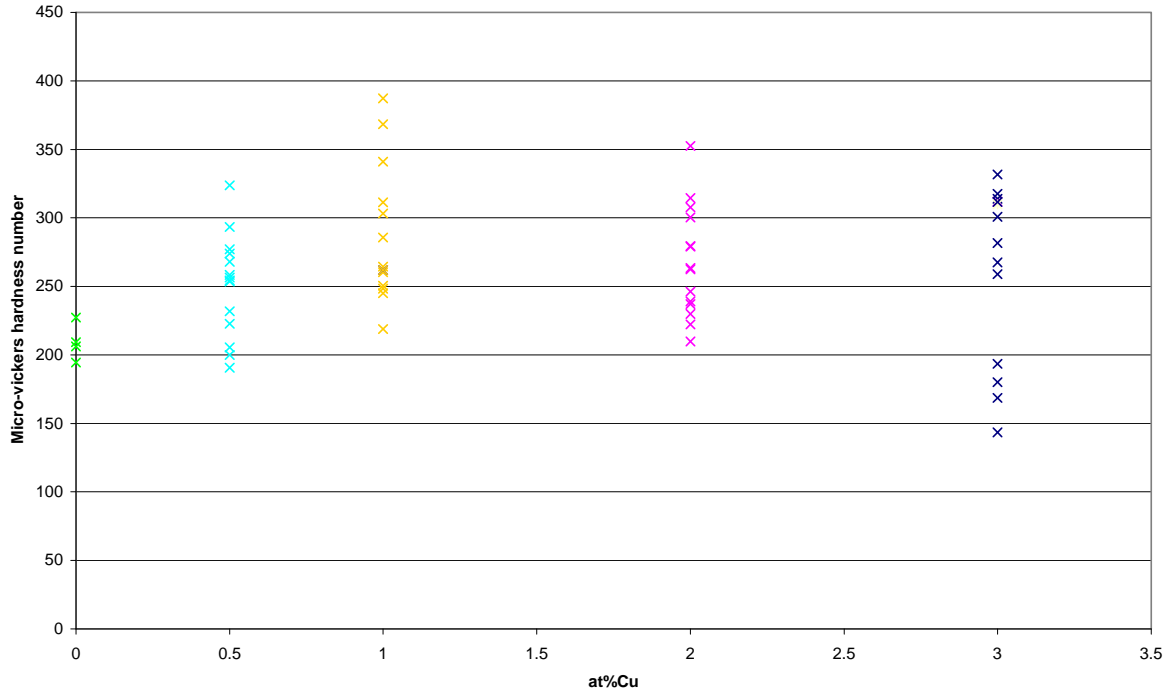


Figure 29 Comparison of micro-vickers hardness number for Pd-8at%Y-Cu alloys

The results of these measurements for Pd-8at%Y and the Pd-Y-Cu series are shown in Figure 29 above. The results for Pd-8at%Y show an agreement with those given Fort et al.³⁸ (Figure 30) who found Pd-8at%Y to have a Vickers hardness number (V.H.N) of 240 after an anneal at 750 °C for 6 hrs, and 180 V.H.N in the hydrogenated condition. After homogenisation our Pd-8at%Y sample had been hydrogenated, although in addition rolling and annealing had occurred, so the hydrogen content of the material may have been altered.

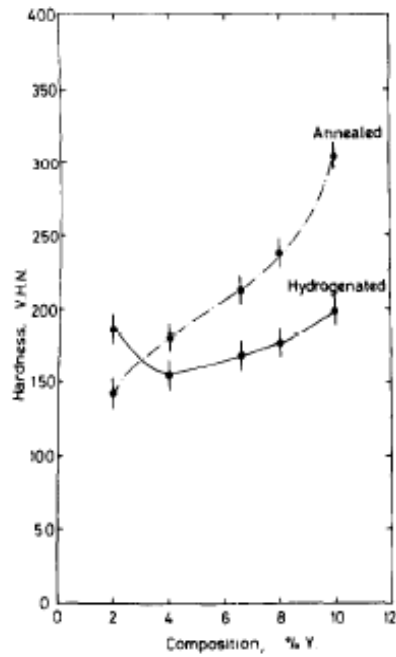


Figure 29 Vickers hardness for Pd -Y in annealed and hydrogenated conditions³⁸.

Taking a larger number of hardness measurements for the same membrane still gave a large range in the results and did not give a narrower point for which most results were concentrated. However, the range seems to be consistently spread for all the samples in the ternary Pd-Y-Cu series so the average of the results was plotted (Figure 31).

As expected from the ease of fabricating the membranes, the Pd-8at% Y-0.5at% Cu alloy was the softest of the four alloys. The Pd-8at% Y-6at% Cu and Pd-8at% Y-10at% Cu were not tested for hardness as the production of these membranes had suggested they would be excessively brittle making them unsuitable. A wider variation in hardness results for these materials would be expected as there are two separate phases present.

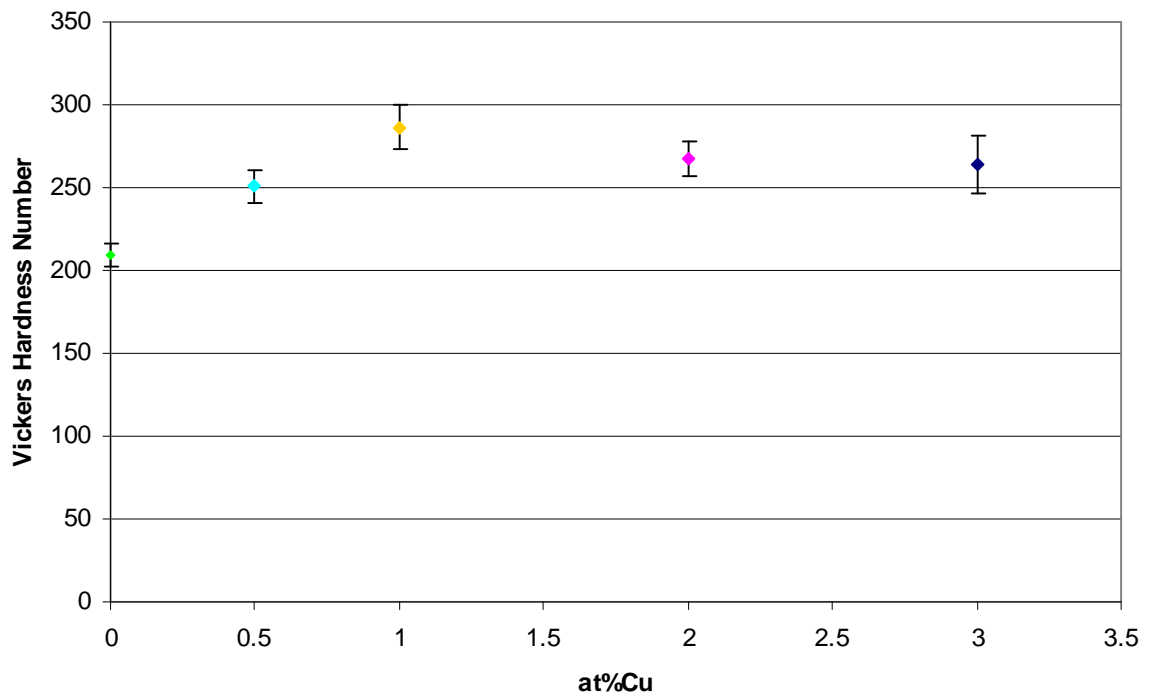


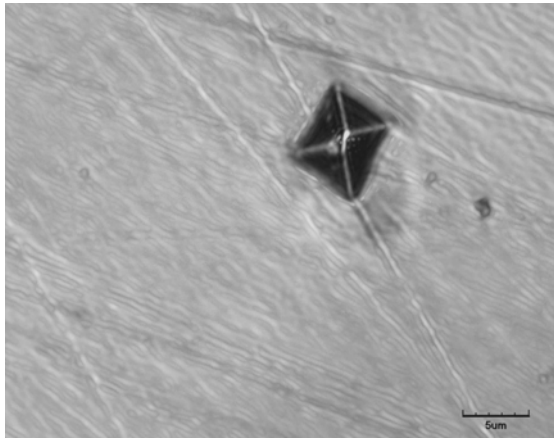
Figure 30 Average Vickers Hardness Number for Pd-Y-Cu series

Plotting the average hardness test results of the four Pd-Y-Cu and the Pd-Y alloys (Figure 31) it can be seen that the addition of 0.5at%Cu produces a smaller increase in hardness than for 1, 2 and 3at%Cu additions (Figure 31). Error bars were used to represent the spread of data within one standard error about the mean.

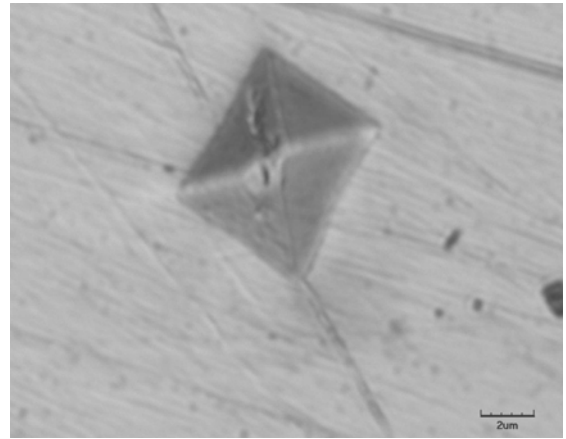
Due to the large variation in Vickers hardness values (Figure 29) for each of the tested alloys further analysis was carried out using a confocal laser microscope to analyse the volumes of the indent created by the diamond indenter.

The samples were examined using the T.V mode on the confocal microscope to find the indents that had been made using the Vickers hardness tester. The microscope mode was then altered to confocal mode and the indents were then further magnified and imaged in 3D mode, and measurements were made to allow the volume to be calculated. The variation in width of

the indents (Figure 32) of approx $8\mu\text{m}$ may partially explain why there was such a large variation in the observed hardness results.



(scale bar = $5\mu\text{m}$)



(scale bar = $2\mu\text{m}$)

Figure 31 Confocal laser microscope images of the indents made using a micro-vickers hardness tester

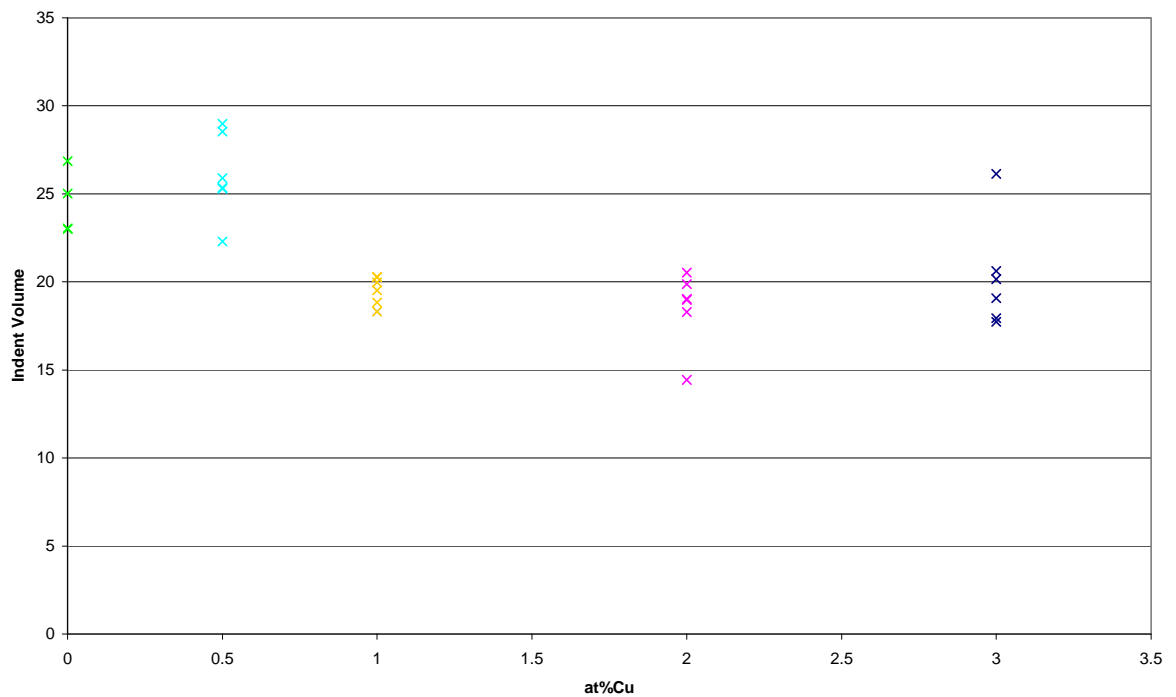


Figure 32 Volume results for Vickers hardness test indents for Pd-Y-Cu series

The results from analysing the volumes (Figure 33) of the indents appear to agree with those results for the VHN numbers (See Figure 29). As expected, the softer materials have a larger indent volume as the indent would be deeper. Some of the spread in the results appears to have been reduced although, compared to using only Vickers hardness values, there is still a significant spread in the results. This could, however, be linked to the local variations in composition and hence hardness across the material. A further factor which may have affected the results is that the surface of the material is not completely flat leading to varying heights of the indent edges. Tilt correction was carried out to try and eliminate this from the results.

Hardness results for the Pd-23at%Ag alloy showed an average Vickers hardness number (V.H.N) of 108 V.H.N indicating the material is considerably softer than the Pd-Y-Cu series for which the Vickers hardness numbers are at least double that of the silver alloy. The average hardness for the Pd-40wt%Cu alloy of 163 V.H.N is midway between the hardness of the Pd-23at%Ag and Pd-8at%Y alloy.

4.5 Microstructural/ Micrographic Analysis

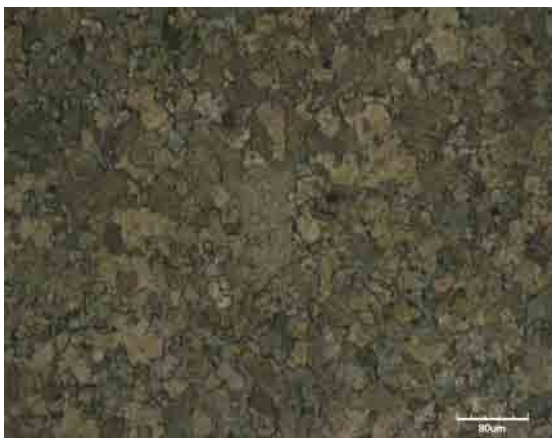
Etching of the samples was carried out before they were placed under the confocal microscope to examine the variations in the grain structure between the different alloys in both the rolled and annealed conditions. The etchant of 30% nitric acid mixed with 70% water had been identified as suitable for palladium and palladium alloys⁶⁴. However, the literature had not indicated the etching time required for each sample.

The mounting of two samples together in the same polymer mount was found to be problematic. Even though each mount contained alloys of the same composition, one sample

was in the rolled condition the other was in the annealed condition. In most cases it was found that one sample would etch quicker than the other, causing problems in trying to optimise the etching time to gain clear images of each sample under the microscope.

The Pd-40wt%Cu was etched first. As this alloy has the lowest palladium content, the alloy became over-etched in less than 10 sec. This meant that clear images of this alloy were only gained in the annealed condition (Figure 34). Both images of this alloy showed large variations in colour contrast. The higher magnified image showed this variation within the individual grains. These became further apparent when looking at the alloy under non-confocal mode (Figure 35). The differences in appearance of these grains could be linked to the differences in structures present in this alloy which contains both f.c.c., and b.c.c. phases.

It was only possible to gain limited images for the Pd-40wt%Cu alloy due to the faster than expected rate at which it etched. This meant it was not possible to get images for this alloy in the rolled condition, due to the limited time left to complete the process and the need to prepare the sample again after it had become over etched.

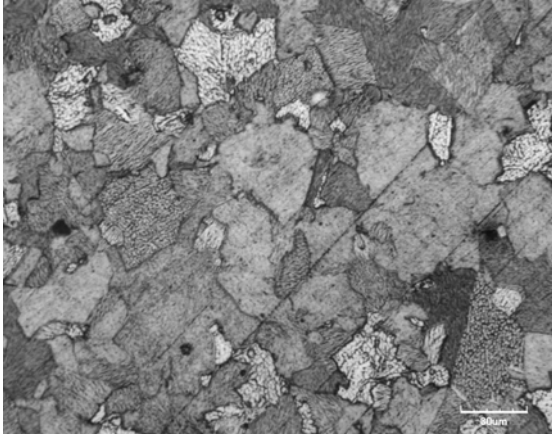


(scale bar = 80 μm)



(scale bar = 30 μm)

Figure 33 Confocal microscope images of Pd-40wt%Cu, annealed, etched in 30% nitric acid at 70°C



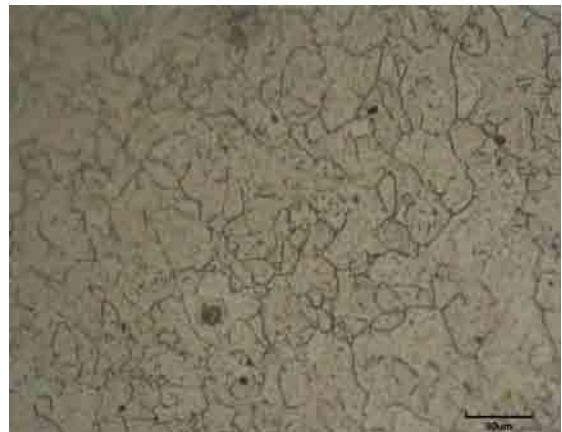
(scale bar = 30 μm)

Figure 34 Confocal micrograph image
Pd-40wt%Cu in non-confocal mode

Of all the alloys etched, the clearest images were gained for the Pd-23at%Ag alloy (Figure 36, Figure 37) the small broken grains (Figure 36) are coalesced by annealing at 750 °C for 6 hrs with the recrystallisation of the grains clear in the annealed sample (Figure 37). The variation of colour across the sample is not as apparent as in the Pd-40wt%Cu alloy, although some areas do appear paler than other areas.



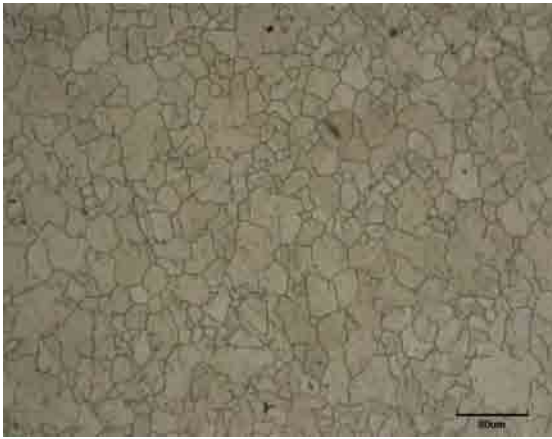
(scale bar = 80 μm)



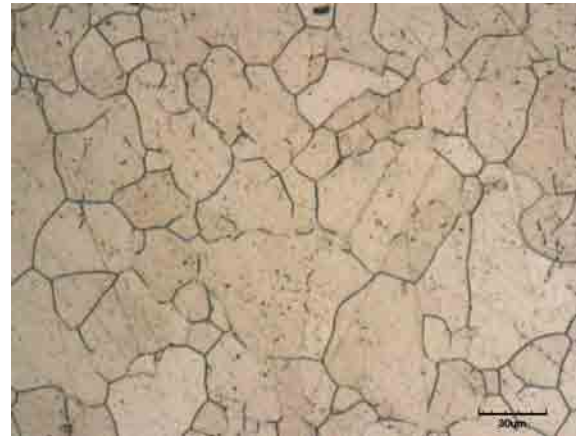
(scale bar = 30 μm)

Figure 35 Confocal microscope images of Pd-Ag rolled. Etched in 30% Nitric acid solution at 70°C

The annealing of the Pd-23at%Ag alloy results in a variation in the grain size (Figure 37) of the alloy. The larger grains average approximately 30 μm across, and were surrounded by a large amount of smaller grains of approximately 15 μm across.



(scale bar = 80 μm)



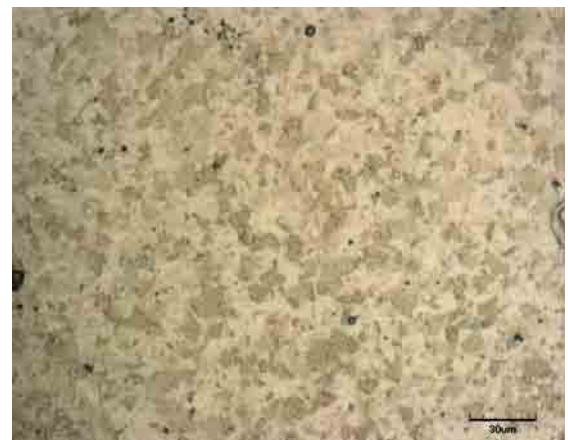
(scale bar = 30 μm)

Figure 36 Confocal microscope images of Pd-Ag alloy after annealing at 750°C for 6 hours. Etched in 30% nitric acid solution

The Pd-8at%Y images (Figure 38 and Figure 39) show some variations in colour, although not the same as the copper alloy. Although the grains are apparent in these samples, the grain boundaries are not as clear as those seen in the Pd-23at%Ag alloy.



(scale bar = 80 μm)



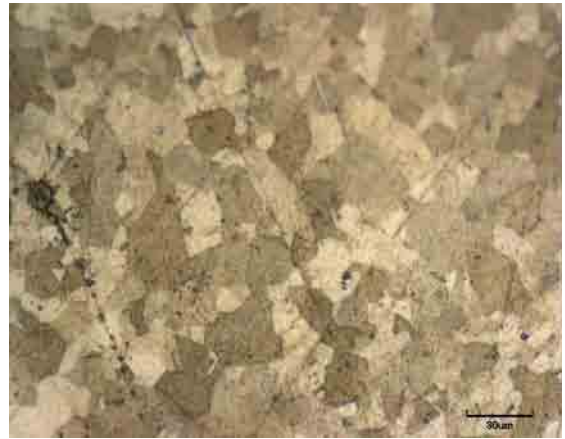
(scale bar = 30 μm)

Figure 37 Confocal microscope images of Pd-8at%Y rolled, etched in 30% nitric acid solution

The grain size of the annealed Pd-8at%Y alloy is more uniform than for the Pd-23at%Ag alloy, averaging 25 μ m in diameter (Figure 39)



(scale bar = 80 μ m)



(scale bar = 30 μ m)

Figure 38 Confocal microscope images of Pd-8at%Y annealed at 750°C for 6 hours, etch in 30% nitric acid solution.

The four ternary alloys took a much longer time to etch with the Pd-8at%Y-0.5at%Cu alloy requiring around 4 minutes in the etchant. After 4 minutes, etching time some grains were starting to appear, although the complete grain structure had not become clear. Further etching was not possible as the Bakelite mount had started to crumble. This suggests a different etchant maybe required for the successful optical imaging of the ternary alloys.

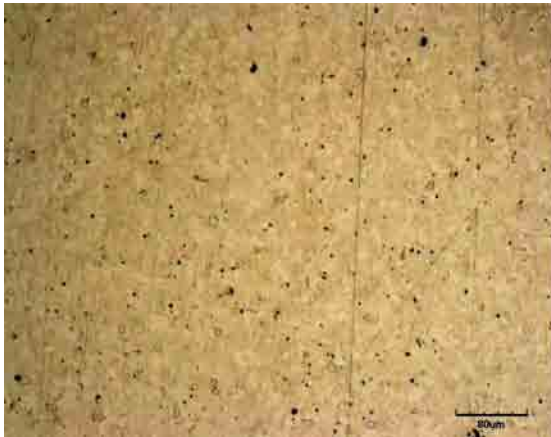


(scale bar = 80 μ m)

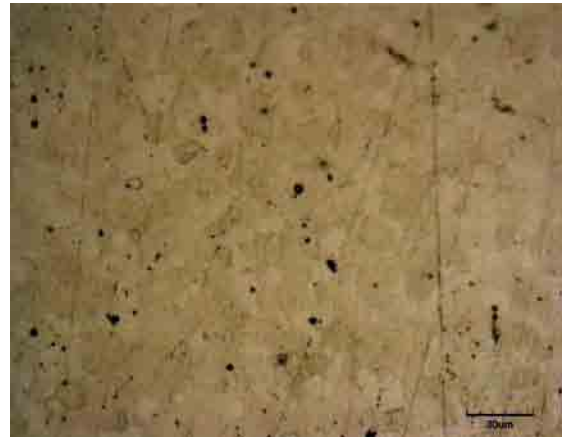


(scale bar = 30 μ m)

Figure 39 Confocal microscope images of Pd-8at%Y-3at%Cu, rolled, etched in 30% nitric acid solution at 70°C

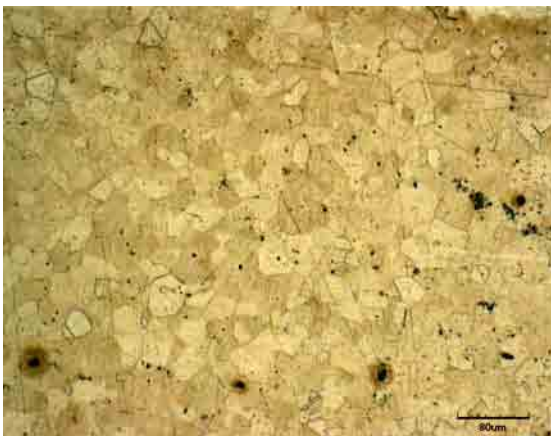


(scale bar = 80 μm)

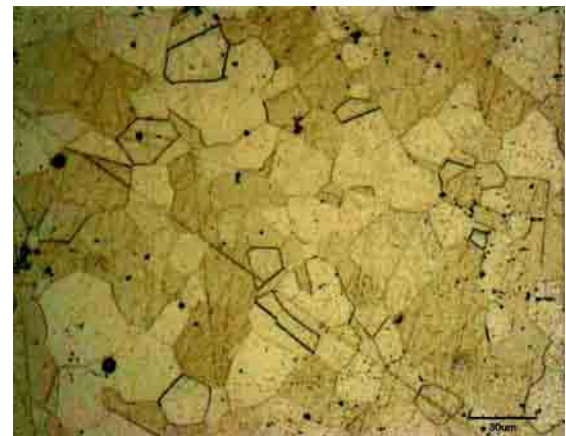


(scale bar = 30 μm)

Figure 41 Confocal microscope images of Pd-8at%-2at%Cu, rolled, etched in 30% nitric acid solution at 70°C



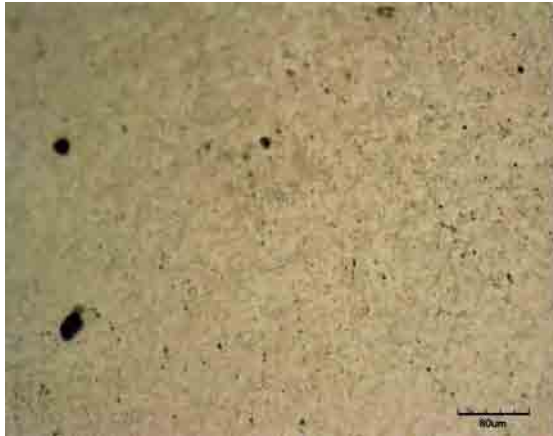
(scale bar = 80 μm)



(scale bar = 30 μm)

Figure 40 Confocal microscope images Pd-8at%Y-2at%Cu annealed, etched in 30% nitric acid at 70°C

The grains in the annealed Pd-8at%Y-2at%Cu (Figure 42) and Pd-8at%Y-1at%Cu (Figure 44) can be clearly seen, with the boundaries of some individual grains much clearer than others. The reason for this is unclear, but it could possibly be linked to local variation in the copper concentration.

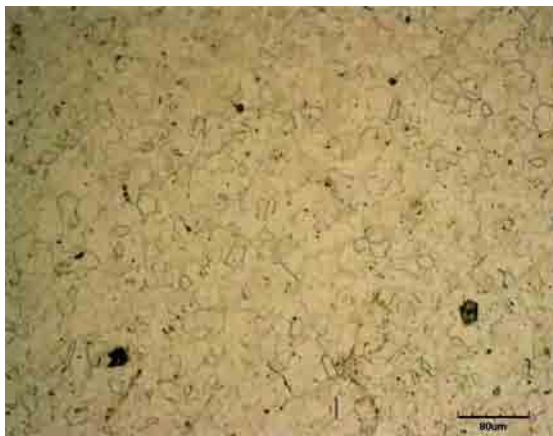


(scale bar = 80 μm)



(scale bar = 30 μm)

Figure 41 Confocal microscope images of Pd-8at%Y-1at%Cu, rolled, etched in 30% nitric acid at 70°C



(scale bar = 80 μm)



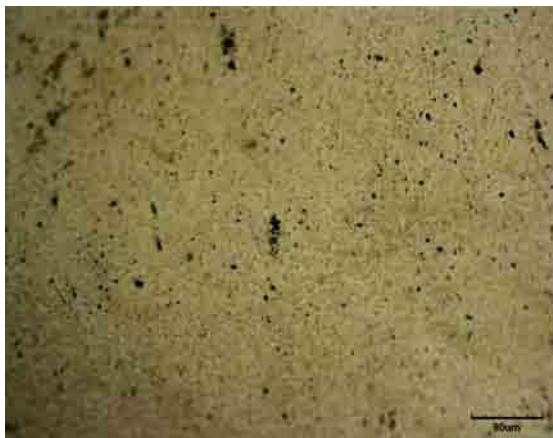
(scale bar = 30 μm)

Figure 42 Confocal microscope images for Pd-8at%Y-1at%Cu, annealed, etched in 30% nitric acid at 70°C

In comparing the annealed images for the Pd-8at%Y-2at%Cu (Figure 42) alloy and the Pd-8at%Y-1at%Cu (Figure 44) alloy, the grains appear to be generally smaller in the Pd-8at%Y-1at%Cu alloy, approximately 10-15μm in width compared to approximately 20-25μm for the Pd-8at%Y-2at%Cu alloy. There also appear to be more variation in colour contrast between the grains in the Pd-8at%Y-2at%Cu alloy.

The grain structure for the Pd-8at%Y-3at%Cu (Figure 40) could not be imaged clearly although the grains appear to be smaller than those of the of the Pd-8at%Y-2at%Cu (Figure 41) and Pd-8at%Y-1at%Cu alloys (Figure 43), and more consistent in size across the alloy.

The effect of the nitric acid solution on the bakelite mount caused crumbling and some solution after exposure for the etch time required for the Pd-8at%Y-0.5at%Cu sample. This affected the flatness of the sample remaining in the bakelite, leading to poorly focussed images of the samples surface. Images of this sample are therefore not completely focused across the whole observed field (Figure 45-Figure 46).

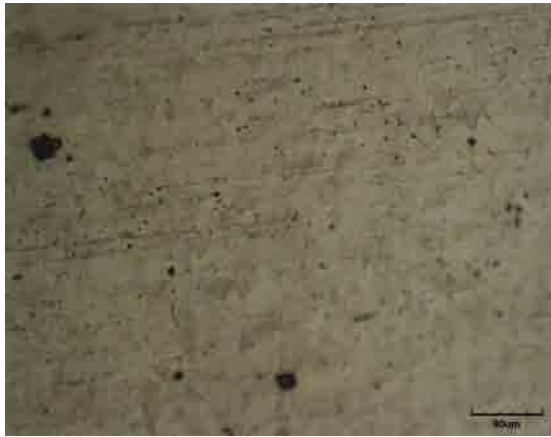


(scale bar = 80 μm)



(scale bar = 30 μm)

Figure 43 Confocal microscope images for Pd-8at%Y-0.5at%Cu rolled, etched in 30% nitric acid at 70°C



(scale bar = 80 μm)



(scale bar = 30 μm)

Figure 44 Confocal microscope images for Pd-8at%-0.5at%Cu annealed, etched in 30% nitric acid at 70°C

The images of the Pd-8at%-0.5at%Cu again show variations in the grain size across the sample, although the grains appear to be smaller in general, averaging 10μm diameter. The grains are smaller than those observed in the binary Pd-8at%Y alloy.

4.6 HYDROGEN FLUX

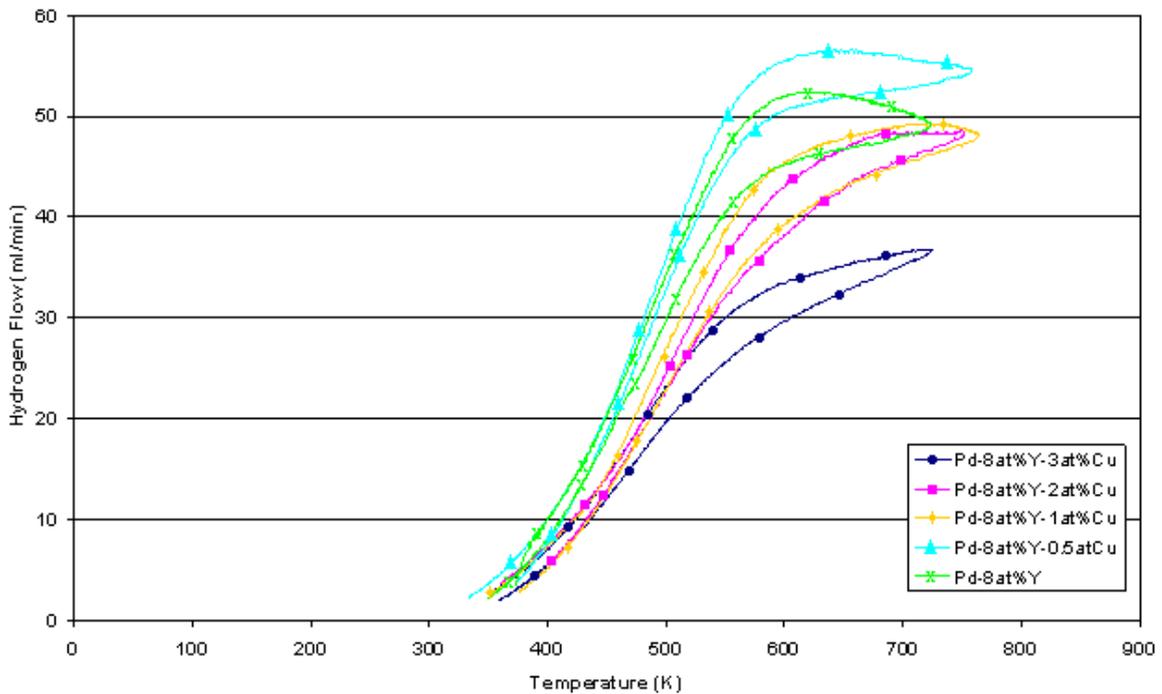


Figure 47 Comparison of hydrogen flow data for Pd-8at%Y, Pd-8at%Y-0.5at%Cu, Pd-8at%Y-1at%Cu, Pd-8at%Y-2at%Cu and Pd-8at%Y-3at%Cu

The hydrogen flow data for a Pd-8at%Y membrane and the four alloys in the Pd-Y-Cu series are plotted as a function of absolute temperature in Figure 47. Hydrogen flow was measured with increasing membrane temperature until flow rate reached a maximum and started to decrease, temperature was reduced back to the starting flow rate. The results show that all of the alloys reach a maximum hydrogen flow rate at different temperatures and that the maximum hydrogen flow value is also dependant on alloy composition. The previously tested (under standard conditions) Pd-8at%Y (included in Figure 47) alloy reaches a maximum H_2 flow of 52.4 ml/min at a temperature of 610K.

The H_2 flow results for the series of Pd-Y-Cu alloys demonstrate that the Pd-8at%Y-0.5at%Cu has the highest hydrogen flow values of all the alloys, reaching a

maximum of 56.5ml/min at 632.9K. Maximum hydrogen flow values then generally decrease as the copper content of the alloy increases. Maximum H₂ flow of 49.2ml/min is reached at 717K, for the Pd-8at%Y-1at%Cu alloy, whereas for the Pd-8at%Y-2at%Cu alloy, maximum flow is 48.67 ml/min at 748.9K and for the Pd-8at%Y-3at%Cu alloy it is 36.78 ml/min at 714.8K.

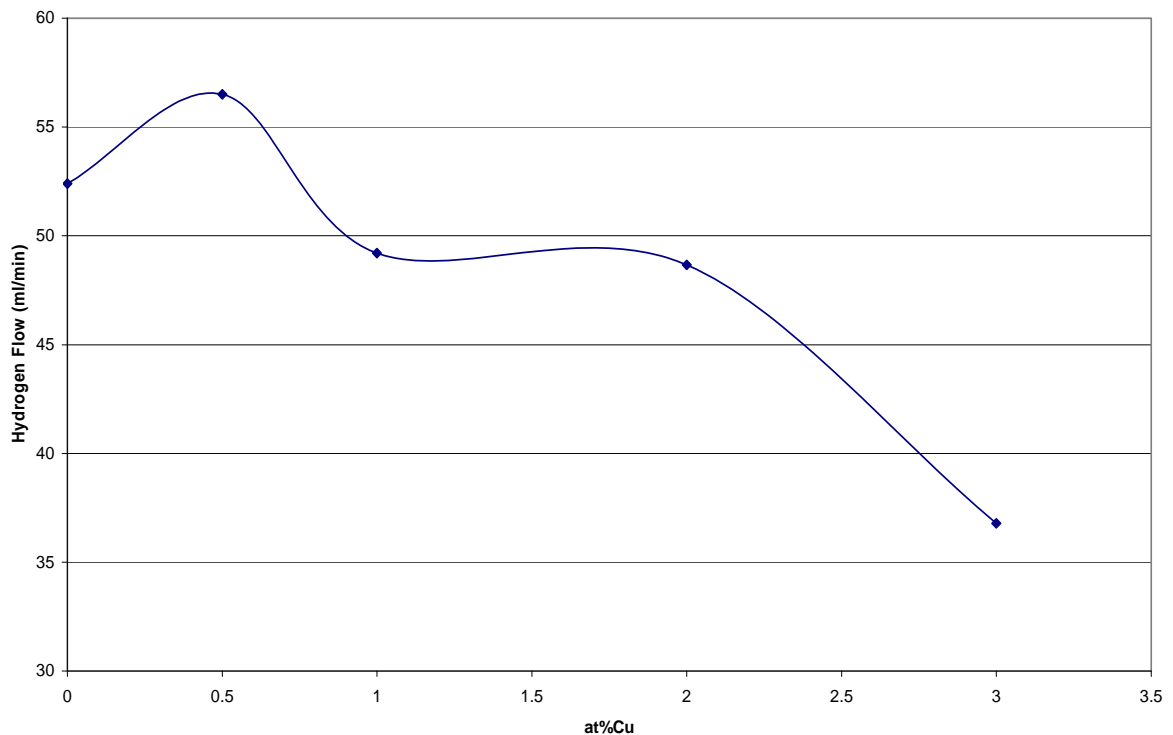


Figure 48 Maximum hydrogen flow verses Cu concentration

The curve in Figure 48 shows how increasing the copper content of the Pd-8at%Y-Cu alloy affects hydrogen flow, results clearly show that the hydrogen flow is improved by the addition of a small amount of copper, but for concentrations greater than 0.5 at% there is no further improvement in hydrogen flow.

4.7 COST ANALYSIS

Palladium is an expensive metal although the cost of palladium membranes maybe reduced though alloying with metals such as silver, yttrium and copper. The cheapest alloys are therefore those with a high copper content, as copper is significantly cheaper than any of the other useable alloying metals. A cursory analysis has been made of the membranes tested in this project based on the current cost of the materials when currently purchased from Sigma Aldrich⁶⁵.

Table 13 The cost of Palladium, Yttrium, Copper and Silver Sigma Aldrich prices Sept 2008)

	Weight Purchased (g)	Cost (inc. VAT) (£)	Cost per gramme (£/g)
Palladium Wire (1mm diameter)	9	408.9	45.43
Yttrium Ingot	10	70.85	7.09
Copper Wire (1mm diameter)	70	57.58	0.82
Silver Wire (2mm diameter)	4.1	61.45	14.99

Calculations have been standardised to cost/gramme to allow for a fair comparison between all materials. Calculations were made based on the amount of material required to make five times the amount required for one disc membrane (diameter 21mm) when rolled to 200 μm in thickness.

Table 14 Summary of costs for membranes produced

Alloy		Palladium	Yttrium	Copper	Silver	Total
Pd	Weight (g)	4.164				4.164
	Cost (£)	189.17				189.17
Pd ₇₇ Ag ₂₃	Weight (g)	3.097			0.938	4.035
	Cost (£)	140.70			14.06	154.76
Pd ₉₂ Y ₈	Weight (g)	3.687	0.268			3.955
	Cost (£)	167.50	1.90			169.4
Pd _{91.5} Y ₈ Cu _{0.5}	Weight (g)	3.67	0.268	0.012		3.95
	Cost (£)	166.73	1.90	0.01		168.64
Pd ₉₁ Y ₈ Cu ₁	Weight (g)	3.652	0.268	0.024		3.944
	Cost (£)	165.91	1.90	0.02		167.83
Pd ₉₀ Y ₈ Cu ₂	Weight (g)	3.617	0.269	0.048		3.934
	Cost (£)	164.32	1.91	0.04		166.27
Pd ₈₉ Y ₈ Cu ₃	Weight (g)	3.582	0.269	0.072		3.923
	Cost (£)	162.73	1.91	0.06		164.7
Pd ₈₆ Y ₈ Cu ₆	Weight (g)	3.476	0.270	0.145		3.891
	Cost (£)	157.91	1.91	0.12		159.94
Pd ₈₂ Y ₈ Cu ₁₀	Weight (g)	3.334	0.272	0.243		3.849
	Cost (£)	151.46	1.93	0.20		153.59
Pd ₆₀ Cu ₄₀ *	Weight (g)	2.4		1.6		4.000
	Cost (£)	109.03		1.31		110.34

* All research on PdCu alloys has been made using weight % rather than atomic % so for comparison in this table the amounts of palladium and copper required for a 4 g sample have been made.

Table 14 shows how the biggest reduction in cost is seen in the Pd-40wt%Cu alloy due to this alloy having the largest amount of palladium being replaced by the cheapest of the three alloying elements. Although the next cheapest alloy is then the Pd-8at%Y-10at%Cu this alloy has been identified as unsuitable for this application due to fabrication difficulties. The Pd-23at%Ag, is almost 19 % cheaper than the pure palladium required for the same membrane, whereas the Pd-8at%Y-0.5at%Cu alloy is 11 % cheaper than for pure palladium. It should be noted that whilst the Pd-8at%Y-0.5at%Cu is more expensive than Pd-23at%Ag the hydrogen throughput is greater and will probably require less material to give equivalent membrane performance in terms of hydrogen flow.

4.8 General Discussion

The addition of copper to a Pd-8at%Y membrane has been shown to affect several key membrane properties. The effects of increasing Cu alloying additions are more apparent on some membrane characteristics than others, leading to non-linear variation of lattice spacings, initial increases in hardness and reduced hydrogen flow.

Comparing the lattice spacings of the Pd-8at%Y alloy and the Pd-8at%Y-Cu series shows that the initial small additions of copper increase the lattice spacings of the alloy reaching a maximum at 1at%Cu before the lattice spacing is then reduced. Similar variations are seen in the variation of hardness with copper composition. The Vickers hardness for the Pd-8at%Y-1at%Cu alloy was the highest, with Pd-8at%Y-2at%Cu and Pd-8at%Y-3at%Cu being lower.

In addition to hardness, the strength of a material is linked to the materials grain size, with the materials strength generally increasing with decreasing grain size according to the Hall-Petch relationship⁶⁶. Grain boundary analysis of the alloys in this work indicate the Pd-8at%Y-0.5at%Cu alloy maybe has the smallest sized grains, suggesting this alloy should exhibit the greatest strength.

This measure of strength of the membrane is important, as a stronger membrane will last longer during cycling, however, for the membrane to be most effective we need to combine membrane strength with ductility and ease of fabrication.

The hydrogen flow vs Cu composition for Pd-Y-Cu alloys reaches a maximum for Pd-8at%Y-0.5at%Cu, then decreases with increasing copper content. Although hydrogen flow for the Pd-8at%Y-1at%Cu and Pd-8at%Y-2at%Cu alloys is approximately 13% lower than the Pd-8at%Y-0.5at%Cu alloy, the values for the two alloys are almost identical. This suggests that hydrogen flow is linked to both copper content of the alloy and the number of grain boundaries contained in the material.

In terms of raw materials, the cheapest Pd-8at%Y-Cu alloy fabricated for this project was Pd-8at%Y-10at%Cu alloy although the properties of this alloy make it unsuitable for hydrogen purification membrane applications. The cost of Pd-Y-Cu alloys slowly increases as the copper content decreases, with the Pd-8at%Y-0.5Cu alloy the most expensive in the Pd-8at%Y-Cu series as it contains the most palladium. This alloy is nevertheless marginally cheaper than the Pd-8at%Y alloy. The large amount of silver that replaces the palladium in the Pd-23at%Ag alloy makes this cheaper than the Pd-Y alloys.

Materials cost has been examined for small-scale samples in this project. However when looking at materials for industrial applications (section 2.3.1.1), a number of other factors must be considered and not just the basic cost of the initial metallic alloy constituents.

The Pd-8at%Y-0.5at%Cu alloy also shows the best hydrogen flow of the alloys tested in this project, with hydrogen flow values also greater than those for Pd-25at%Ag found by Fort et al.³⁸ This, along with the increased strength of the material and easier fabrication due to addition of the small amount of copper, means that further research into the alloy properties would be justified. One of the most interesting aspects to investigate would be the effect of

hydrogen sulphide on H₂ flow through this membrane, as research has shown the addition of copper to palladium can improve the resistance to poisoning by H₂S, which isn't seen in other palladium alloys.

5.0 CONCLUSIONS

This study has shown that the effect of copper additions on a Pd-8at%Y alloy leads to marked changes in a number of key alloy parameters relevant to membrane performance. Small additions of copper create a single phase f.c.c solid solution material. Continued additions of copper above 3at% leads to the formation of a secondary f.c.c. phase (Pd_3YCu) between 3at% and 6at%Cu. This secondary Pd_3YCu phase makes the material brittle and the continued formation of this phase with increasing copper content creates a material that cannot be rolled to the required 100 μm membrane thickness, and so would not be usable for the required application.

When comparing the results of this research to previous phase diagrams^{59 60}, it can be seen that these results more closely agree with the results by Kotur et al.⁵⁹

Although all the Pd-Y-Cu alloys samples were prepared with a target composition of 8at%Y, EDS showed that variations can be seen in yttrium content in all four of the samples in the Pd-8at%Y-Cu series. The Pd-8at%Y-1at%Cu and Pd-8at%Y-0.5at%Cu are near to 8at%, on average. However, yttrium content of Pd-8at%Y-2at%Cu was higher, averaging at ~9at%Y. In contrast, the yttrium content of Pd-8at%Y-3at%Cu appears to be lower (below 7.5%) in all but one case, and below 7at%Y in seven different areas of measurement (EDS).

The hardness of the alloys is not a linear function of increasing Cu compositions. With small additions of copper the hardness initially increases Pd-8at%Y-1at%Cu. Hardness then appears to decrease as copper content of the material exceeds 1%.

The grain size of the different alloys also appears to vary with Cu content, generally increasing as the copper content increases.

The addition of a small amount of copper (0.5at%Cu) to Pd-8at%Y increases the rate of hydrogen flow through the membrane from 52.4 to 56.5 ml/min. However, increasing the copper content beyond 0.5% starts to then reduce the rate of hydrogen flow.

Taking all the above points into consideration, the Pd-8at%Y-0.5at%Cu may well be the most cost efficient material to use for membrane fabrication. Besides the increase in strength and ease of rolling, the material could allow for thinner membranes to be produced than those tested here. The thinner membranes may also be tested at higher pressures allowing for greater hydrogen flow through the material. The increased strength should also improve the length of time they can be used in service. However, before any firm conclusions can be made, further research needs to be carried out, on a number of issues raised by the present work.

Table 15 Summary of results for the PdYCu alloys tested

Target Composition	Composition (EDS)	Lattice Parameter (Å)	Hardness (VHN)	Average Grain Size (µm)	Rate of H ₂ flow (ml/min)
Pd-8at%Y	-	3.946	209.3	25	52.4
Pd-8at%Y-0.5at%Cu	91.8% Pd 7.8% Y 0.4% Cu	3.9624	250.7	10	56.5
Pd-8at%Y-1at%Cu	91% Pd 8% Y 1% Cu	3.964	286.3	10-15	49.2
Pd-8at%Y-2at%Cu	88.8% Pd 9% Y 2.5% Cu	3.9573	267.4	20-25	48.67
Pd-8at%Y-3at%Cu	89.6% Pd 7% Y 3% Cu	3.9486	263.6	-	36.78
Pd-8at%Y-6at%Cu		3.892			
Pd-at%8Y-10at%Cu		3.881			

6.0 FURTHER WORK

- EDS analysis showed that the composition of the majority of the as melted/rolled samples were altered slightly compared to their target gravimetric compositions. Altering the homogenisation conditions of the samples, either for an extended time at the same temperature or at a higher temperature for the same period of time, should give improved homogenisation. This would help to eliminate the variations in results, due to the compositional fluctuations (and not just linked to areas of the sample which had not become homogenised.)
- Further work needs to be carried out on the H₂ flow performance of the Pd-Y-Cu membranes. The membranes need to be tested under cycling of hydrogen, different hydrogen pressures, and in H₂ with a H₂S concentration as low as 50 ppm. At present, most of the membranes have only been tested once for their hydrogen flow characteristics.
- Improved hardness measurements, need to be made testing the samples in the 'as produced' condition, after homogenisation and with the possibility of the button only being rolled twice to ensure the sample is flat before polishing. Testing thicker samples after a number of rolls and after being annealed would also allow for more accurate hardness results to be obtained. Using a thicker sample would allow for a larger load to be applied to the sample when testing, giving a larger indent and therefore more consistent results for the materials hardness.

- Electrical resistivity tests may help to detail the distribution of copper in the alloys, in particular showing whether it is distributed at the grain boundaries. This could shed further light on the significant property changes produced for small Cu additions to Pd-8%at%Y.
- Further investigation of the microstructure of the material needs to be carried out with greater control of the etching conditions. This would allow for more defined grain boundaries when looking at the material under the Confocal microscope. It would also be useful to look at the samples after mounting them separately to get clearer images and to look at the cross section of the material to help investigate grain growth.
- The use of Transmission Electron Microscopy (TEM) could give a further, more in depth analysis of the samples, being used to identify crystal orientation and electronic structure of the samples

REFERENCES

-
- ¹ The Department for Business Enterprise and Regulatory Reform. **Energy White Paper: Meeting the energy challenge**. Chapter 5 pg 127 [online] (2007) [Cited 2009 Sept 20] Available at URL <http://www.berr.gov.uk/energy/whitepaper/page39534.html>
- ² N. Louth The return of king coal. Money Week [online] (2006) [Cited 2009 Sept 6] Available from URL <http://www.moneyweek.com/investments/commodities/the-return-of-king-coal.aspx>
- ³ Department for Business, Enterprise & Regulatory Reform **Energy Trends** (March 2008) [Cited 2008 June 15] Available at URL <http://www.decc.gov.uk/en/content/cms/statistics/publications/trends>
- ⁴ The Department for business Enterprise and Regulatory Reform. **Energy White Paper: meeting the energy challenge**. Chapter 4-Oil, gas and coal. [online] (2007) [Cited 2009 Sept 20] Available at URL <http://www.berr.gov.uk/energy/whitepaper/page39534.html>
- ⁵ J. Anderson and C. D. Anderson (2005) **Electric and Hybrid Cars: A History**. McFarland.
- ⁶ G.Walker (University of Queensland) Lecture: Hybrid Electrical Vehicles Meet the Electricity Grid Plug in Hybrids (PHEVs) and Vehicle to Grid (V2G) [Cited 2009 Sept 20] Available at URL http://www.itee.uq.edu.au/~walkerg/pickup/V2G_2_GRW.ppt#287.1
- ⁷ R. Harris, D. Book, P. Anderson, and P. Edwards Hydrogen Storage the Grand Challenge *The Fuel Cell Review* (2004) 17-23
- ⁸ Hydrogen Fact Sheet, Hydrogen Production- Steam Methane Reforming (SMR) New York State Energy Research and Development Authority [online] [Cited 2009 Sept 20] Available at URL <http://www.getenergysmart.org/files/hydrogeneducation/6hydrogenproductionsteammethanereforming.pdf>
- ⁹ Climate Technology Sheet #9 Hydrogen Production Climate Action Network Europe [online] (2003) [Cited 2009 Sept 24] Available at URL http://www.climnet.org/CTAP/techsheets/CTAP09_H2Production.pdf
- ¹⁰ Hydrogen Fuel Cell Engines and Related Technologies - Module 3 Hydrogen use in Internal Combustion Engines [online] (2001) [Cited 2009 Sept 24] Pub College of the Desert Energy Technology Training Centre Available at URL http://www1.eere.energy.gov/hydrogenandfuelcells/tech_validation/pdfs/fcm03r0.pdf
- ¹¹ D.Book Lecture notes Hydrogen Production, Hydrogen and Fuel Cells Module, University of Birmingham (2008)
- ¹² Hydrogen Fuel Cells [online] (2008) [Cited 2009 Sept 20] Available at URL http://www1.eere.energy.gov/hydrogenandfuelcells/pubs_educational.html
- ¹³ X. Cheng, Z. Shi, N. Glass, L. Zhang, J.Zhang, D. Song, Z.S. Liu, H. Wang, J. Shen A review of PEM hydrogen fuel cell contamination: Impacts, mechanisms and mitigation. *Journal of Power Sources* **165** 2007 739-756
- ¹⁴ G.J. Grashoff, C.E. Pilkington, C.W. Corti The purification of hydrogen: A Review of the technology emphasising the current status of palladium membrane diffusion. *Platinum Metals Review* **27** (4) (1983) 157-169
- ¹⁵ A. Walton Lecture notes Porous materials for hydrogen storage and purification, Hydrogen and Fuel Cells Module, University of Birmingham (2008)

-
- ¹⁶ D. Book, A. Walton, V. Mann, J. Speight, R. Harris Hydrogen Storage and Purification Research University of Birmingham Available at URL http://www.ierp.bham.ac.uk/documents/res_MMH2.pdf (2010)[Cited 2010 May 16]
- ¹⁷ C. Nishimura, M. Komaki, S. Hwang, M. Amano V–Ni alloy membranes for hydrogen purification *Journal of Alloys and Compounds* **330–332** (2002) 902–906
- ¹⁸ M. Amano, M. Komaki and C. Nishimura Hydrogen permeation characteristics of palladium-plated V-Ni alloy membranes *Journal of the Less-Common Metals*, **172-174** (1991) 727 731
- ¹⁹ Kitco [online] (2008) [Cited 2008 March]
Available from URL <http://www.kitco.com/charts/livepalladium.html>
- ²⁰ S. N. Paglieri and J. D. Way Innovations in Palladium membrane research. *Separation and Purification methods* **31**(1) (2002) 1-169
- ²¹ A. G. Knapton Palladium Alloys for Hydrogen Diffusion Membranes A Review Of High Permeability Materials. *Platinum Metals Review* **21**(2) (1977) 44-50
- ²² D Edlund Hydrogen Separation and purification using dense metallic membranes. DOE Hydrogen Separation Workshop [online](2004) [Cited 2009 Sept 16]
Available from URL http://www1.eere.energy.gov/hydrogenandfuelcells/pdfs/separ_07_atomic_edlund.pdf
- ²³ R.G. Musket Effects of contamination on the interaction of hydrogen gas with palladium: A review. *Journal of the Less Common Metals* **45** (1976) 173-183
- ²⁴ H. Gao, Y. S. Lin, Y. Li, B. Zhang Chemical Stability and Its Improvement of Palladium-Based Metallic Membranes. *Industrial and Engineering Chemistry Research*. **43** (2004) 6920-6930
- ²⁵ H. Amandusson, L.G Ekedahl, H. Daaetun Hydrogen permeation through surface modified Pd and PdAg membranes. *Journal of Membrane Science* **193** (2001) 35-47
- ²⁶ M. Kajiwara S. Uemiya, T. Kojima Stability and hydrogen permeation behavior of supported platinum membranes in presence of hydrogen sulphide. *International Journal of Hydrogen Energy* **24** (1999) 839-844
- ²⁷ R.C Hurlbert, J.O. Konecny Diffusion of hydrogen through palladium. *Journal of Chemical Physics* **34** (1961) 655
- ²⁸ A. Kulprathipanja, G. O. Alptekin, J. L. Falconer, J. D. Way Pd and Pd-Cu membranes: inhibition of H₂ permeation by H₂S. *Journal of Membrane Science* **254** (2005) 49-62
- ²⁹ Metals and Materials Science, processes, applications R.E Smallman and R.J. Bishop publisher Butterworth and Heinmann
- ³⁰ Magnetron Sputtering [online] [cited 2009 Sept 27] Available from URL <http://www.teercoatings.co.uk/index.php?page=magsput>
- ³¹ Autocatalytic (Electroless) plating [online] [Cited 2009 Sept 27] Available from URL <http://www.efunda.com/processes/surface/electrolessplatings.cfm>
- ³² Plating [online] [Cited 2009 Sept 27] Available from URL http://en.wikipedia.org/wiki/Electroless_plating#Electroless_plating
- ³³ J. B. Hunter Silver-palladium film for hydrogen separation (1956) United States Patents Office Patent 2,773,561

-
- ³⁴ H. Amandusson, L. G. Ekedant, H. Dannetun Hydrogen permeation through surface modified Pd and PdAg membranes *Journal of Membrane Science* **193** (2001) 35-47
- ³⁵ D.Fort and I.R. Harris The physical properties of some palladium alloy hydrogen diffusion membrane materials. *Journal of the Less Common Metals* **41** (1975) 313-327
- ³⁶ J. Okazaki, D. A. Pacheco Tanaka, M. A. Llosa Tanco, Y. Wakui, F. Mizukami, T. M. Suzuki Hydrogen permeability study of the thin Pd-Ag alloy membranes in the temperature range across the α - β phase transition *Journal of Membrane Science* **282** (2006) 370
- ³⁷ H. Yoshida, S. Konishi and Y. Naruse. Effects of impurities on hydrogen permeability through palladium alloy membranes at comparatively high pressures and temperatures *Journal of the Less-Common Metals*, **89** (1983) 429 - 436
- ³⁸ D.Fort, J. P. G. Farr and I. R. Harris A comparison of palladium-silver and palladium-yttrium alloys as hydrogen separation membranes. *Journal of the Less common metals*. **39** (1975) 293-308
- ³⁹ M. L. H. Wise, I. R. Harris and J.P.G. Farr X-Ray studies of the α/β miscibility gaps of some palladium solid solution-hydrogen systems. *Journal of the Less Common Metals* **41** (1975) 115-127
- ⁴⁰ D. T. Hughes and I. R. Harris A comparative study of hydrogen permeabilities and solubilities in some palladium solid solution alloys. *Journal of the Less Common Metals* **61** (1978) P9-P21
- ⁴¹ I.R. Harris and M.Norman The electronic state of cerium in some palladium alloys. *Journal of the Less Common Metals* **15** (1968) 285-298
- ⁴² J. R. Hirst, M. L. H. Wise, D. Fort, J. P. G. Farr and I. R. Harris Hydrogen softening in some palladium-rare earth solid solution alloys. *Journal of the Less Common Metals* **49** (1976) 193-211
- ⁴³ M. L. Doyle, and I. R. Harris Palladium-Rare Earth Alloys Their Order-Disorder Transformations and Behaviour With Hydrogen. *Platinum Metals Review* **32** (3) (1988) 130-140
- ⁴⁴ D.T. Hughes, J.Evans and I.R. Harris The influence of order on hydrogen diffusion in the solid solution alloys Pd-5.75at%Ce and Pd-8at%Y. *Journal of the Less Common Metals* **74** (1980) 255-262
- ⁴⁵ R.C. J. Wileman and I. R. Harris The permeability behaviour of protium and deuterium through a Pd-7.5at% Y membrane. *Journal of the Less-Common Metals*, **109** (1985) 367 – 374
- ⁴⁶ K. S. Rothenberger, B. H. Howard, R. P. Killmeyer, M. V. Ciaocco, B. D. Morreale, R. M. Enick Palladium-Copper Alloy Membrane Performance Under Continuous H₂S Exposure [online] [Cited 2009 Sept 24] Available from URL http://www.netl.doe.gov/technologies/hydrogen_clean_fuels/refshelf/papers/hydrogen/PDCuMembranePerformance.pdf
- ⁴⁷ Method for hydrogen separation and purification U.S Patent 3,439, 474 (1969)
- ⁴⁸ P. M. Thoen, F. Roa, J. D. Way High flux palladium-copper composite membranes for hydrogen separations. *Desalination* **193**(1-3) (2006)224-229
- ⁴⁹ A. Kulprathipanja, G. O. Alptekin, J. L. Falconer, J. D. Way Pd and Pd-Cu membranes: inhibition of H₂ permeation by H₂S *Journal of Membrane Science* **254** (2005) 49-62
- ⁵⁰ K. S. Rothenberger, B. H. Howard, R. P. Killmeyer, M. V. Ciocco, B. D. Morreale, R. M. Enick Palladium-Copper alloy membrane performance under continuous H₂S exposure US Department of Energy
- ⁵¹ L. Karakaya and W.T. Thompson The Ag-Pd (Silver-Palladium) System *Bull. Alloy Phase Diagrams* **9**(3) (1988) 237-243

-
- ⁵² W. G. Moffatt (1976) **The Handbook of Binary Phase Diagrams** General Electric. Vol.1-.5 New York Schenectady
- ⁵³ H. K. D. H. Bhadeshia Solid Solutions: The Hume-Rothery Rules University of Cambridge [online] (2004) [Cited 2009 Sept 24] Available from URL <http://www.msm.cam.ac.uk/phase-trans/2004/titanium/hume.rothery.html>
- ⁵⁴ I. R. Harris and M. Norman Observations on the lattice spacings of some α Pd-X solid solutions and some Pd₃X phases *Journal of the Less Common Metals* **22** (1970) 127-130
- ⁵⁵ Y. Sakamoto, F.L. Chen, M.Furukawa and K.Mine The (α - β) hydrogen miscibility gaps in hydrogenated palladium-rich Pd-Y(Gd)-Ag ternary alloys. *Journal of the Less Common Metals* **166** (1990) 45-56
- ⁵⁶ Y. Sakamoto, F.L. Chen, M.Furukawa and M. Noguchi. Permeability and diffusivity of hydrogen in palladium-rich Pd-Y(Gd)-Ag ternary alloys *Journal of Alloys and Compounds* **185** (1992) 191-205
- ⁵⁷ Y. Sakamoto, F.L. Chen, Y. Kinari Permeability and diffusivity of hydrogen through Pd-Y-In(Sn, Pb) alloy membranes *Journal of Alloys and Compounds* **205** (1994) 205-210
- ⁵⁸ F. L. Chen, Y. Kinari and Y. Sakamoto The α - β hydrogen miscibility gaps in hydrogenated Pd-Y-In(Sn, Pb) ternary alloys. *Journal of Alloys and Compounds* **205** (1994) 119-124
- ⁵⁹ B. Ya. Kotur, H. Michor, E.Bauer, G.Hilscher The Y-Cu-Pd ternary system at 600°C (0-25 at% Y): a reinvestigation. *Journal of Alloys and Compounds* **296** (2000) 285-289
- ⁶⁰ P. Villars, A. Prince, H. Okamoto (1995) **Handbook of ternary phase diagrams** ASM International
- ⁶¹ S. Fletcher PhD Project University of Birmingham (2008)
- ⁶² R. B. Carmona-Benítez Synthesis and Characterisation of Pd-based alloys for use in Dense-Metal hydrogen purification membranes. MRes Thesis, University of Birmingham (2008).
- ⁶³ S.Fletcher, V. Mann Hypnomem project University of Birmingham
- ⁶⁴ W. F. Gale and T.C Totemeier (2004) **Smithells Metals Reference Book** Elsevier
- ⁶⁵ Sigma Aldrich [online][Cited 2008 Sept 29] Available from URL <http://www.sigmaaldrich.com/united-kingdom.html>
- ⁶⁶ Grain Boundary Strengthening [online] [Cited 2009 Aug 6] Available from URL <http://en.wikipedia.org/wiki/Hall-Petch>